DSN Radio Science System Design and Testing for Voyager-Neptune Encounter

N. C. Ham, T. A. Rebold, and J. F. Weese
Telecommunications Systems Section

The DSN Radio Science System presently implemented within the Deep Space Network was designed to meet stringent requirements imposed by the demands of the Voyager-Neptune encounter and future missions. This article elaborates on one of the initial parameters related to frequency stability. It describes the requirement, specification, design, and methodology for measuring this parameter. It also includes the description of special instrumentation that was developed for the test measurements and initial test data resulting from the system tests performed at Canberra, Australia and Usuda, Japan.

I. Introduction

The Voyager-Neptune encounter and new deep space missions have imposed very stringent requirements upon the Deep Space Communications Complex (DSCC) Radio Science System, and have prompted a new design to meet these demands. The design requirements apply not only to the basic system, but also to the test methodology and instrumentation necessary to test and verify the system's performance at the complexes. This article describes some of the parameters that were critical to the design, the design configuration, and the test methodology and instrumentation. Presented are results of initial measurements performed at the Canberra Deep Space Communications Complex (CDSCC) and the Deep Space Tracking Complex in Usuda, Japan. The Usuda facility consists of the associated 64-meter antenna, which will gather radio science data from the Voyager 2 spacecraft for post-encounter data correlation with the CDSCC 70-meter antenna. The CDSCC antenna receives S-/X-band data and Usuda receives data at S-band.

Short-term and long-term frequency stability are two of the critical parameters that demanded extra attention. The long-term stability is important to enhance the correlation efficiency of the received data from the separate facilities as one factor and for spacecraft orbit tracking measurements as another. The short-term or phase-noise spectral density characteristics of the receiving system are important to permit the reception of the spacecraft's radio-frequency carrier signal which contains basic scientific information after occulting the medium. This phase-noise parameter is related to the Radio Science System's inherent reference frequency source and the complementary active circuit elements which process and utilize this signal.

It is important that the received carrier signal which contains radio science data in the form of its amplitude, phase, and frequency perturbations not be contaminated, degraded, or masked by the receiving and data acquisition system. Analysis of the carrier used by some of the spacecraft radio science

experiments utilizes the perturbation of the dual radio frequency (RF) signals (S-/X-band) traveling between the spacecraft and the ground tracking antennas to study the aspects of the planetary system visited, as well as other nonplanetary phenomena of interest.

Spacecraft radio science comprises two broad categories of investigation:

1. Occultation measurements of the radio signal as it passes through and probes the media of interest (planetary atmosphere, ionosphere, and rings) while the spacecraft is on the far side of the planet.
2. Tracking measurements wherein the perturbations of the spacecraft orbit are analyzed for information on gravity or other effects [1].

A stabilized frequency reference source on board Voyager 2, called an ultra-stabilized oscillator (USO), is used for generating the dual S- and X-band RF signals and achieves its maximum stability over time intervals of 1 to 600 seconds. This permits the use of a one-way downlink mode of transmission and reduces any discontinuity in the transmitted signal versus time. It is apparent that the ground radio science receiving and data acquisition system must possess greater stability than the USO, both in the short and long term, to maintain suitable accuracy in the radio science measurements. The use of hydrogen-maser frequency standards in the ground systems provides long-term frequency stability; however, careful design and special emphasis are required to maintain this long-term capability and to ensure good short-term stability as well.

The short-term stability can also be defined in the frequency domain as the phase-noise spectral density distribution (or spectrum) about the carrier signal. The Voyager 2 USO possesses good phase-noise spectral density for frequencies offset from the carrier 1 Hz to 10,000 Hz. These good characteristics aided the collection of Saturn ring data [1].

As a result of differential frequency shifts from different parts of the rings, ring occultation signals arrive at the Earth receivers with a frequency spectrum which is broadened by this interaction. Figure 1(a) shows the relative positions and motion of the spacecraft, planetary ring, and Earth, with the resulting spectrum of the received signal. The geometry of ring occultation is shown, with the signal on a direct and indirect path to Earth. Figure 1(b) displays the power spectrum of the received X-band signal when Voyager 1 was behind the midpoint of Saturn's Ring A. Primary features of this spectrum are the well-defined spectral line at the free-space frequency, corresponding to the direct spacecraft-to-Earth ray path, the broad irregular distribution of energy over a range of frequencies, corresponding to scattered waves, and the noise floor [1].

II. Ground System Design Requirements

The noise-power spectral density characteristics of the Earth receiving and data acquisition system should be considerably better than the spacecraft signal, so that the system's contributing noise floor does not mask the spectrum of the received signal during the process of frequency downconverting the carrier to a low-frequency video-band signal for digitization and data acquisition by tape recording.

Similarly, the long-term frequency stability should be adequate to maintain accuracy in the radio science measurements. The Voyager-Neptune encounter requirement for this is specified in terms of the square root of the Allan variance as 6×10^{-13} for 1-second integration time (τ) reducing to 3×10^{-13} as a function of $1/\tau$ at 10 seconds and remaining at this value out to 1000 seconds.

The ground receivers produce two basic noise sources which compete against the received spacecraft signal. One is the thermal noise source and the other is the previously discussed phase noise. The thermal noise is due mainly to the RF-input low-noise amplifier (LNA) with additional contributions by the antenna microwave losses and atmospheric elements. The phase noise is contributed largely by the receiver's first local oscillator (LO), which is derived from the hydrogen-maser frequency standard of the frequency and timing subsystem (FTS).

Figure 2 is a model of the spacecraft signal and the noise sources and illustrates the manner in which the spacecraft signal-to-noise ratio (SNR) is degraded before the final data acquisition process by the radio science receiving system.

The spacecraft transmits a carrier signal, P_c, with an inherent short-term stability phase noise, $\sigma_{\phi sc}$. The term widely used for describing and quantifying this parameter is the phase-noise spectral density as a function of the sideband frequencies offset from the carrier $\mathscr{L}(f_m)$ in the frequency domain. Its magnitude is expressed as the single-sideband (SSB) phase-noise power density divided by the carrier power in dBc/Hz, or

$$\mathscr{L}(f_m) = \frac{\text{Power Density (SSB)}}{P_c} \qquad \text{(dBc/Hz)}$$

where f_m is the offset frequency away from the carrier.

This is an indirect measure of the noise energy easily related to the RF power spectrum on a spectrum analyzer. $\mathscr{L}(f_m)$ is defined as the ratio of the power in one phase-modulation sideband on a per-hertz basis to the total signal power. Phase noise can also be viewed as a continuous spectrum of infinitely

close phase-modulation sidebands and can be derived from the spectral density of phase fluctuations using phase modulation theory.

As shown in Fig. 2, the carrier power is reduced by the space loss to the ground receiver; however, the inherent phase-noise density to carrier power ratio remains the same as it appeared at the spacecraft's transmitter output except for perturbations created by the media intervening between the spacecraft and the receiver. The resultant carrier power thermal SNR referenced to the receiver input is related to this resultant carrier power and the thermal-noise spectral density N_o of the receiving system, or

$$\mathrm{SNR}_T = \frac{P_c'}{N_o}$$

This thermal-noise spectral density in first-order terms is related to the receiver elements by the expression

$$N_o = kT_{op} = k\left[T_{\mathrm{LNA}} + \frac{T_{\mathrm{MIXER}}}{\mathrm{POWER\ GAIN}_{\mathrm{LNA}}}\right]$$

ignoring antenna microwave noise/losses and follow-on receiver noise contributors appearing as additive noise. However, the phase-noise contribution to the received signal by the receiver is a multiplicative effect. Since the phase noise was considered to be random phase fluctuation modulation, the spacecraft signal can be expressed as

$$A_c \sin\left[\omega_c t + \Delta\phi_c(t)\right]$$

where $\Delta\phi_c(t)$ represents random phase fluctuations. Similarly, the receiver first LO signal can be expressed as

$$V_{\mathrm{LO1}}(t) = A_{\mathrm{LO}} \sin\left[\omega_{\mathrm{LO1}} t + \Delta\phi_{\mathrm{LO1}}(t)\right] \qquad (1)$$

with $\Delta\phi_{\mathrm{LO1}}(t)$ representing random phase fluctuations of the receiver LO.

These signals are multiplied at the receiver first mixer to produce the first intermediate frequency (IF):

$$V_{\mathrm{IF}}(t) = A_{\mathrm{IF}} \cos\left[\omega_{\mathrm{IF}} t + \Delta\phi_c(t) + \Delta\phi_{\mathrm{LO1}}(t)\right] \qquad (2)$$

where the phase fluctuations are assumed Gaussian and are independent.

Equation (1) shows that the phase fluctuation modulation of the first LO signal creates sideband variance in proportion to its magnitude A_{LO1}. When multiplied to the carrier signal, as shown by Eq. (2), the resultant IF magnitude $A_{\mathrm{IF}} = A_c A_{\mathrm{LO1}}/2$ to sideband variance ratio will be in the same relative ratio as the LO signal to its sideband variance. The overall resultant ratio, however, will be the root-sum-square (RSS) of the carrier and LO sideband variances. Stated another way this means that the receiver phase-noise spectral-density $\mathscr{L}(f_m)$ value contributed by the first LO is transferred to the resultant IF signal in the same ratio independent of the carrier magnitude A_c and the resultant IF signal phase noise is the RSS of the spacecraft carrier and first LO variances. Analogous to an amplitude SNR, the phase-noise spectral density SNR of the output signal can be expressed as

$$\sigma\mathrm{SNR(PHASE)} = \frac{\dfrac{\sigma^2_{\phi_{sc}}}{P_c}}{\dfrac{\sigma^2_{\phi_{RS}}}{P_{\mathrm{LO}}}} = \frac{\mathscr{L}_{sc}(f_m)}{\mathscr{L}_{RS}(f_m)}$$

and ideally then

$$\mathscr{L}_{RS}(f_m) \ll \mathscr{L}_{sc}(f_m)$$

Other important continuous noise and unwanted line-spectral signal effects due to the local oscillator are the random amplitude fluctuations and line-spectral interference (or spurious sideband signals). Extending Eq. (1), the instantaneous output voltages of the first LO signal can be written as

$$V_{\mathrm{LO1}}(t) = \left[A_{\mathrm{LO1}} + \delta\epsilon(t)\right] \sin\left[\omega_{\mathrm{LO1}} t + \Delta\phi_{\mathrm{LO1}}(t)\right]$$

where $\delta\epsilon(t)$ is the instantaneous amplitude fluctuation of the signal. The spectral density $S_{\delta\epsilon}(f)$ of the signal amplitude fluctuations follows the same derivation as the spectral density of phase fluctuations. The amplitude modulation (AM) noise components are typically much less than the phase-noise components; however, it is important that the AM noise be measured or verified to ensure that it is not a major contributor. The amplitude-noise modulation is in phase to LO signal phase while the phase-noise modulation is in quadrature phase to the LO signal phase.

The unwanted line-spectra sideband signals are more deterministic compared to the continuous random noise fluctuations. These are commonly defined as spurious frequencies and will also appear as both amplitude and phase-modulation sidebands. These line-spectra spurious frequencies can generally be identified, but it is difficult to locate their source. They are largely related to power-line frequency and are intermodulation products of the various mixers and frequency-multiplier circuits.

If the spurious sideband signals are at the power-line frequency fundamental they are probably intruded into the receiving system by magnetic coupling via a power transformer to unshielded components and by electrostatic-type coupling, and also via ground-loop currents due to improper grounding of sensitive and weak signal paths.

If the spurious signals appear as harmonics of the power-line frequencies, they can be traced to the DC power supply if they are of the straightforward line-frequency rectification and filtering type.

As opposed to the RSS combination of the random noise fluctuations, these line-spectra spurious sidebands combine directly in all of the various possible LO paths and appear at the final video-frequency output terminal as the aggregate net summation of their amplitude and phases. It is obvious that every LO signal path could potentially be the carrier of these spurious sideband signals; however, since the first LO chain possesses the highest frequency-multiplication factor, this is the first suspected path of spurious frequency intrusion.

For example, the reference signal for the first LO chain which contains spurious frequency intrusion creates an equivalent phase modulation which can be expressed as

$$V_{\mathrm{LO}_{\mathrm{REF}}}(t) = A_{\mathrm{LO}_{\mathrm{REF}}} \sin\left[\omega_{\mathrm{LO1}_{\mathrm{REF}}} t + m_p \sin \omega_{\mathrm{SPUR}} t\right] \tag{3}$$

where $\omega_{\mathrm{LO1}_{\mathrm{REF}}} t$ is the reference input signal to the first LO chain, $\omega_{\mathrm{SPUR}} t$ is the spurious modulating signal, and m_p is the equivalent modulation index of the spurious intrusion. Expanding Eq. (3) and expressing in terms of the Bessel functions, it can be shown that the spectrum consists of the LO signal acting as the carrier plus sidebands related to the sum and differences of the spurious signal to the LO carrier, whose amplitudes are various-order Bessel functions of m_p. As this phase-modulated wave is frequency multiplied to a higher frequency (to the desired first LO injection frequency), the effect is to increase the modulation index by a factor equal to the frequency-multiplication value. If the first-order sideband spurious signal has a specific value of $\mathscr{L}(f_m)$ dBc/Hz, its value after multiplication will change by the factor 20 log N. For example, if the reference signal contains a spurious signal of -90 dBc/Hz and is frequency multiplied by X81, then the resultant first-order sideband spurious value at the multiplier output is degraded by 38 dB or to a value of $\mathscr{L}(f_m)_{\times 81}$ = -52 dBc/Hz due to the frequency multiplication only. The frequency-multiplier circuits themselves can also develop spurious signal intrusion which would modify the output value depending upon the effective m_p and the relative phase of the spurious signals.

This is similarly applicable to the random or continuous spectrum modulation signal (phase noise) in that the $\mathscr{L}(f_m)$ value is degraded proportional to the multiplication factor N.

Thus, Eq. (3) can be written with a multiplication factor N as

$$V_{\mathrm{LO}_{\mathrm{REF}}}(t) = A_{\mathrm{LO}_{\mathrm{REF}}} \sin N\left[\omega_{\mathrm{LO1}} t + m_p \sin \omega_{\mathrm{SPUR}} t\right]$$

and the effective modulation index is increased by Nm_p resulting in an increased sideband amplitude proportional to N at the multiplied output frequency sin $\omega_{\mathrm{LO1}} t$.

The system specification for the Voyager-Neptune encounter phase-noise spectral density and spurious signal magnitude is -53 dBc/Hz at f_m = 1 Hz and -60 dBc/Hz at 10 Hz continuous from 1 Hz to 10 kHz for the X-band channels, and -45 dBc/Hz at f_m = 1 Hz continuous to 10 kHz for the S-band channels. The lower value specifications of -60 and -45 dBc/Hz were limited by the expected received spacecraft carrier power to thermal-noise SNR for the respective channels.

III. System Design and Configuration

This section describes the implemented Radio Science Systems for the DSCC and Usuda, Japan configurations in support of the Voyager-Neptune encounter.

A. Deep Space Communications Complex Configuration

Figure 3 is the block diagram of the Radio Science System configuration for DSCC-10, DSCC-40, and DSCC-60. The system has the capability to receive simultaneously S- and X-band frequencies from a spacecraft at the normal DSN RF-assigned channels at the 11/3 S-/X-band frequency ratio, or either channel individually from a 70-meter antenna. Similarly, right circular polarization (RCP) and left circular polarization (LCP) of RF or individual channels can be received simultaneously. Not shown in the diagram is the capability to receive simultaneously a single X-band and a single S-band RF channel from the 34-meter High-Efficiency Antenna at each DSCC by switching the IF signal into the RF-IF converter via the IF distribution and gain-normalizer assembly shown in the diagram.

The output of the 70-meter antenna S-/X-band polarizers feeds two RF X-band and two S-band LNAs comprising traveling-wave masers (TWMs), which in turn drive the RF-IF converters of the Radio Science System. This converter assembly converts the RF signal to the IF by the first LO frequencies

of 8100 and 2000 MHz. This X-band first LO signal path with the ×81 and ×5 frequency multiplication from the phase calibration generator (PCG) 20-MHz output signal and the PCG reference signal from the FTS hydrogen-maser primary frequency standard are critical in meeting the previously mentioned frequency-stability parameter requirement.

The PCG is a phase-conjugation circuitry which stabilizes the phase characteristics of the long transmission line from the FTS to the antenna and essentially transfers the longterm frequency stability of the hydrogen maser to the antenna cone area. The normal function of the PCG circuitry is to provide a comb of very stable frequencies at the input to the TWMs for very-long-baseline interferometry (VLBI) phase calibration [2]. Thus it can provide a stable reference to the first LO multiplier chain to meet the long-term frequency stability requirements. The ×5, which was to provide the 100-MHz reference to the LO frequency multipliers, was not available for the initial installation; thus, the 100-MHz signal was obtained via a long coaxial cable from the FTS for the initial frequencystability measurements. The long-term frequency-stability measurement using Allan variance methodology resulted in the system meeting the requirements for the Voyager-Neptune encounter; therefore, this will be the configuration at the DSCC. For the Galileo mission, which requires a greater frequency stability, the reference from the PCG or another circuitry concept may be used.

To meet the phase-noise spectral density requirements, the 100-MHz input signal to the above coaxial cable was obtained via a 5-MHz phase-locked loop (PLL) located in the FTS. This phase-locked clean-up loop (CUL) contains a very narrow loop bandwidth which improves the phase-noise spectral density at low offset frequencies of the hydrogen-maser output.

The IF signals from the antenna are sent to the Signal Processing Center (SPC) via long coaxial cable transmission lines, buried between the antenna and the SPC and terminated into the IF distribution assembly, which direct the IF signals to the proper IF channels of the radio science IF-VF (RIV) converter or to the VLBI System, which is not shown in Fig. 3. The RF LNA and RF-IF converters are also used for the VLBI system.

The buried IF cables from the antennas and the SPC vary in length due to the physical locations of the antennas from the SPC, which are not standard for the various DSCCs; consequently, the attenuation of the IF signals from the RF-IF converters to the IF distribution and gain-normalizer assembly are of different values around the network. The gain-normalizer function was inserted at this point so that the resultant IF signal amplitude is the same value for all complexes regardless of the antenna signal origin. This standardized the design and the gain profile of the RIV for all the complexes.

The output IF signal from the gain-normalizer assembly is sent to the RIV which heterodynes it to another IF, and finally to an IF of 10 MHz where band-pass filters (BPFs) narrow the bandwidth to the desired value prior to the final downconversion to video-band frequency (VF) for digitization and magnetic tape recording. The heterodyning of the second IF to the RIV is accomplished via a programmable local oscillator (PLO) whose output frequency is programmed by the DSCC processor assembly (DPA) through the programmed oscillator control assembly (POCA). The PLO follows a predicted spacecraft Doppler frequency versus time profile to maintain the received carrier frequency centered within the BPF bandwidth. The PLO is an existing assembly within the DSN with phase-noise spectral density and long-term frequency stability characteristics which meet the error-budget allocation in this function and alleviate the burden to the first LO in meeting the overall system requirement. The PLO was modified to meet the spurious-frequency requirements which were largely related to power-line frequency. The frequency-multiplication and bias-frequency mixers for the PLO normalize the final IF to correspond to the input-RF 11/3 ratio.

Each RIV IF channel contains a set of BPFs which can be selected to meet the particular mission requirements. Four are located at the 10-MHz IF with nominal bandwidths from 2000 to 45,000 Hz, and there are two very narrow-bandwidth BPFs in a 100-kHz IF presently at 82 and 415 Hz. Only one filter can be selected for operation at a time in any of the IF channels, in either a single or paired operational mode. These filters are easily removed and replaced if a mission requires different bandwidths than those initially inserted. The band-pass filtered signal is finally downconverted to a video-band frequency (VF) and sent to the DSCC spectrum processor (DSP) for digitization and tape recording. Each IF channel contains an isolated VF output-signal port available for monitoring or testing.

The DSP utilizes a 24-MHz quartz-crystal PLL for converting an FTS 10-MHz reference signal to the desired analog-to-digital converter (ADC) sampling signals that digitize the VF input signals. The digitized signals are then formatted, multiplexed, etc., and recorded on magnetic tape for the final data acquisition. Any digitized signal that enters the DPA can be converted back to an analog form via a digital-to-analog converter (DAC) which is used for monitoring purposes by the spectral signal indicator (SSI). Similarly, the SSI can output a signal that can be transmitted back to JPL for remote monitoring of the received VF signal. The DAC also provides a 12-parallel data-plus-clock output interface jack for connection to

the digital stability analyzer test instrumentation, which is used at the complex for measuring the total Radio Science System phase-stability performance characteristics.

B. Usuda Configuration

The radio science equipment configured at the Usuda Deep Space Center in Usuda, Japan is the result of a combined effort between JPL and the Japanese Institute of Space and Astronautical Sciences (ISAS). Originally developed to support the Japanese Planet-A spacecraft launched toward Halley's Comet, the Usuda Deep Space Center operates a 64-meter Cassegrainian antenna with a beam waveguide feed. In addition to the antenna, ISAS is also providing the RF-IF converter, the primary data acquisition subsystem (DAS), and the hydrogen-maser frequency standard. JPL is providing the TWM, the Global Positioning Satellite (GPS) receiver, a secondary DAS, and several FTS assemblies.

A block diagram of the Usuda Radio Science System is shown in Fig. 4. Unlike the DSCC implementation, the Usuda system is capable of receiving S-band signals only, although ISAS is planning to upgrade to X-band. Also, the receiver does not decompose the signal into its RCP and LCP components. It is strictly a single-channel system.

The antenna beam waveguide feeds into the JPL TWM which is the primary LNA. Not shown in the figure is the ISAS-provided parametric amplifier (paramp), which is to be used as a backup to the TWM. The system noise temperature using the JPL TWM is about 16.5 kelvins, while the corresponding temperature using the paramp is about 30 kelvins.

The output of the TWM is sent to the ISAS RF-IF converter, which translates the RF center frequency of 2295 MHz down to the IF center frequency of 70 MHz. The RF-IF converter works in two steps, mixing the signal with a first LO of 1880 MHz, then with a second LO of 485 MHz. Since the second LO is higher than the corresponding IF, the polarity of the 70-MHz IF spectrum is inverted with respect to the RF input spectrum.

Following the RF-IF downconversion, the 70-MHz output is sent from the antenna building over a frequency-stable fiber-optic link to the control-room building. Once inside the building the IF signal is filtered to a bandwidth of 7.5 MHz, amplified, and distributed to the two data acquisition subsystems—one supplied by JPL, the other by ISAS.

1. **JPL Data Acquisition Subsystem.** The JPL DAS consists of a RIV and a Mark III occultation data assembly (ODA) that digitizes the video signal, tape records the signal, and controls the LO frequency. The ODA is made up of a Mark III narrow-band occultation converter (NBOC), a Modcomp II computer with an IBM PS/2 computer to provide terminal input, and two Wanco tape drives for recording and storing digitized data. For frequency tuning purposes, the Modcomp II computer accepts and stores 14 point-predict sets entered through the PS/2.

The 70-MHz IF signal enters the JPL RIV, is sent through a 0- to 60-dB variable attenuator (referred to as the RIV attenuator), is then further amplified by 20 dB, and downconverted to the video band of 0 to 40 kHz by a single sideband converter. The local oscillator used is tunable by the ODA computer so that the received spacecraft carrier containing Doppler shift can be kept within the 35-kHz video-frequency filtered bandwidth. The LO mixer injection frequency is derived by frequency multiplying the output of the computer-controlled Dana frequency synthesizer by X4 and then mixing it down with a fixed-frequency 100-MHz signal derived from FTS. This scheme translates the Dana output frequency range of 42 to 43 MHz to cover the desired LO range of 68 to 71 MHz. The tuning capability is provided by the POCA, which takes frequency and ramp-rate commands from the Modcomp II computer and controls and monitors the Dana synthesizer accordingly. In this IF-VF downconversion the local oscillator is again higher in frequency than the IF signal so that the spectrum is inverted once more. Therefore, the spectrum of the video signal, which is recorded onto magnetic tape, is noninverted with respect to the input RF signal.

At the video level, the signal is further amplified, low-pass filtered to a resultant bandwidth of 35 kHz, and then digitized by the NBOC. The video signal can be monitored on a spectrum analyzer at a point just prior to its digitization. Also, a RMS voltmeter is included to measure the level of the signal going into the ADCs in the NBOC. During system precalibrations, the RIV attenuator is adjusted to achieve a video level of about 1 volt RMS in order to avoid saturating the ADCs.

The NBOC digitizes the video signal and sends the data to the Modcomp II computer. It contains four ADCs which are configured to sample the same input signal one at a time each with a phase-shifted sampling signal. Thus, the data stream coming from the four converters is effectively the same as what would come from one converter sampling at four times the rate. To reduce sampling jitter, the sampling signals are derived from a 24-MHz quartz-crystal voltage-controlled oscillator phase locked to an FTS 10-MHz reference signal.

After sampling, the NBOC sends the digitized data to the Modcomp II for magnetic tape recording. The Modcomp II reads each byte immediately after it has been written to the tape and sends the data back to the NBOC. The NBOC then converts the digital data back to an analog signal that can be

monitored with a spectrum analyzer to verify that the desired data are being tape recorded.

2. **ISAS Data Acquisition Subsystem.** The ISAS-provided DAS is the prime recording system, with the JPL subsystem provided as backup. Both subsystems will run concurrently during the encounter.

The two subsystems are functionally equivalent. The ISAS IF-VF converter performs a tuned downconversion with a computer-controlled frequency synthesizer and tape records the signal after digitization. An HP1000/A900 provides the frequency control and data handling, and two Hewlett-Packard tape drives are used for data recording and storage.

The ISAS IF-VF converter differs from the JPL converter in that the first tuned conversion converts the signal to a 20.02-MHz third IF where it is band-pass filtered rather than converted directly to video-band frequency. An additional downconversion translates the carrier to video band, where it is low-pass filtered and amplified prior to digitization. A fast-Fourier-transform (FFT) analyzer monitors the video signal, and a RMS voltmeter facilitates setting the IF attenuator to adjust the video frequency (carrier) to the proper signal level into the ADC.

3. **Frequency and Timing Subsystem.** The frequency and timing subsystem used at Usuda will rely on a hydrogen-maser frequency standard provided by ISAS, which is to be implemented prior to the Neptune encounter. Currently the station reference can be switched between two cesium-beam standards and one rubidium standard. The output of the standard, regardless of type, is sent through a 5-MHz phase-locked CUL to improve the phase-noise spectrum.

The first and second LOs are derived from this 5-MHz output. The 5-MHz signal is frequency multiplied to 100 MHz followed by frequency synthesizers which form 94- and 97-MHz signals that are sent over the fiber-optic link to the RF-IF converter in the antenna building. There the 94-MHz signal is frequency multiplied by 20 and the 97-MHz signal by 5 to provide the first and second LO mixer injection signals.

It can be seen in the block diagram that there are two 5- to 100-MHz X20 assemblies, one from ISAS and one from JPL. The JPL X20 was to provide only a 100-MHz reference signal to the JPL Dana synthesizer third LO chain. The ISAS X20 was the primary 100-MHz source for the first and second LOs; however, during system testing the Allan variance performance was marginal using the ISAS X20, and improved when the 100-MHz reference was derived from the spare JPL X20 assembly. Efforts are underway to modify the JPL X20 assemblies to provide another output port and to improve the ISAS X20 stability. Following final corrections and tests, one X20 reference will be chosen as prime and the other as backup. This is described in more detail in Section V.

IV. System Test Methodology and Plan

The system test plan included the test hierarchy of performing assembly-level tests by the various Cognizant Development Engineers to verify meeting their level of performance requirements and allocated error budget. Similarly, the subsystem was tested at its level to verify the error budget and functional requirements, followed by complete system testing by the System Cognizant Development Engineer.

Figure 5 illustrates the system test concept for measuring the critical phase-noise spectral density and spurious-frequency parameters. Also shown are the special Test Transmitter and phase-noise instrumentation (Digital Stability Analyzer) developed and provided for the system testing. The Stability Analyzer uses digital signal-processing techniques, and in addition to measuring the two parameters, it is capable of measuring the amplitude spectrum, the power spectrum, and the differential phase between any two RIV output channels.

Similarly, the Stability Analyzer has the capability of measuring the long-term frequency stability of both the hydrogen masers and the Radio Science System using Allan variance methodology, which has been universally accepted as a meaningful quantitative measure of fractional frequency deviation [3, 4].

Figure 6 illustrates the relative phase-noise spectral densities of a typical future spacecraft USO, the DSCC Radio Science System, and the special Test Transmitter that formed the basis and concept of testing the Radio Science System for the phase-noise parameter. These values exceed the Voyager-Neptune encounter specifications and illustrate the anticipated requirements for future missions. The Radio Science System was specified as shown to provide ample margin in its performance such that neither the received spacecraft phase-noise floor nor the signal perturbed by the intervening media (or experiment signal) was masked. Similarly, the Test Transmitter must possess better phase noise characteristics than the Radio Science System specification in order to reliably measure the performance.

Figure 7 is the block diagram of the Test Transmitter, which provided phase-coherent S-/X-band output signals with exceptional phase-noise spectral density characteristics. The Test Transmitter was also used for performing long-term frequency-stability tests using Allan variance methodology, whereby a 5-MHz reference signal from the FTS was used to phase-lock the internal primary 5-MHz PLL oscillator. This 5-MHz prime

signal was then allowed to free-run for performing the short-term (phase-noise) frequency-stability tests in the switch position, as shown, to provide the best phase-noise performance. The phase-coherent output signals also permitted measuring the differential phase-stability parameter of the Radio Science System.

Figure 8 is the block diagram of the Usuda test methodology and test instrumentation that were developed and used for the subsystem and system tests. A 10-MHz stable quartz-crystal oscillator (with good phase-noise characteristics) and ×7 multiplier provided the test signal to the DAS at the 70-MHz IF input frequency for measuring the phase-noise spectral density parameter.

A 10-MHz reference signal from the FTS was then switched into the ×7 multiplier to perform the Allan variance measurement. This method was used to test the subsystem at JPL to verify the subsystem performance prior to its installation at Usuda. The instrument for measuring the phase noise/spurious signals is composed of a PLL and an FFT-type commercial spectrum analyzer, while a combination of zero-crossing detector, time-interval counter, and computer processor was used to measure the Allan variance.

Following the installation at Usuda, the subsystem was retested by the same test instrumentation and methodology as performed at JPL prior to its interfacing with the ISAS RF-IF converter. Next, the complete system was tested with the use of the special Test Transmitter as the RF test input signal.

V. System Test Results

This section describes some of the initial system test measurements and results performed at the CDSCC and the Usuda Tracking Station. The Radio Science System measurements were performed at X- and S-band at CDSCC and at S-band at Usuda.

A. DSCC Initial Test Results

Described below are the initial test results performed at CDSCC beginning with the short- and long-term frequency stability data.

Figure 9 shows the Allan variance measurement of the two hydrogen-maser frequency standards. Figures 10(a), 10(b), and 10(c) compare the noise-power spectral density spectra of the two hydrogen masers relative to 10 GHz with the fractional frequency deviation as a function of integration time and spectral density versus offset frequency. The noise-power spectrum plot scales are normalized for phase noise and corrected for sine-wave line-spectra magnitudes. These masers meet the total system Allan deviation specification for the encounter. For the phase-noise spectral density, the system specification is shown corrected for the noise factor and referenced to the 8.4-GHz frequency (the plot is referenced to 10 GHz because of the instrumentation design, and the resultant is for the sum of the two masers; hence, each maser at 8.4 GHz would be approximately –4 dB better than plotted).

Figure 11 shows the Allan variance measurement results at X-band of the total DSS-43 Radio Science System where the Test Transmitter was located within the X-band cone with its 5-MHz reference input obtained from the PCG 20-MHz output via a ×1/4 frequency multiplier. The input 100-MHz signal to the first local oscillator ×81 was obtained from an FTS 100-MHz source fed up to the cone through a hardline coaxial cable. The figure shows that the Voyager system requirement is met with a comfortable margin. If the 100-MHz reference to the ×81 were obtained from a stabilized transmission line (fiber optics, for example), it would shift the plot downward to greater stability and could meet the Galileo requirements of 2.5×10^{-15} for 1000-sec integration. Figure 12 shows the time-residual plot associated with Fig. 11. These plots show only the Radio Science System results since the contribution of the frequency standard is cancelled in the measurement methodology; hence, the total system characteristics must include the sum of these two components.

Figure 13 shows the phase-noise spectral density spectrum of the RIV using a good-quality spectral IF signal input of 300 MHz and the normal Dana POCA as the RIV oscillator. This figure shows the characteristic 60 Hz plus harmonics of the power-frequency spurious signal that had been previously identified during system testing at JPL and Goldstone due to the Dana-POCA combination. These spurious signals were being corrected at the time of these tests by modifications to the Dana-POCA local oscillator.

In the overall Radio Science System, the first and second LOs were identified as the two major contributors to the phase-noise spectral density and spurious signals that appear adjacent to the received spacecraft carrier signal. The first LO and its entire frequency distribution and multiplier chain, originating from the FTS 100-MHz reference signal, is the most dominant of the two sources because of its larger multiplication factor of ×81. The multiplication factor for the second LO is ×11; however, the second LO, comprising the programmable frequency synthesizer (Dana POCA) for tracking the Doppler shift of the spacecraft signal contained large-magnitude power-line spurious signals that required magnetic shielding to meet specifications. The first LO injection signal, occurring at microwave frequencies, was allocated the major portion of the error budget for the phase-noise spectral density. To permit this, an error budget of more than 10 dB below the overall sys-

tem specification was allocated to the second LO. It was seen that the spurious signals of the RIV Dana-POCA combination were above the error budget as shown in Fig. 13; hence, it was necessary to substitute another frequency synthesizer with a better spurious signal response but similar noise-power spectral density characteristics in place of the above combination to better measure and evaluate the first LO contribution to the system phase-noise spectral density and spurious signals. Figure 14 shows the resultant RIV noise-power spectral density/spurious signal characteristics using the Fluke 6160 substitute synthesizer, which was used for the majority of the system tests for determining the first LO contribution.

After considerable system testing, including detailed investigative and probing experiments to isolate the sources of many spurious signal contributors and noise-spectral density degradations, final noise-power spectral density measurements were made. These measurements of the noise-power spectral density were not the desired phase-noise spectral density measurements because the stability analyzer's processing program was erratic in its operation during this time period; the measurements were made with the alternate CDSCC test instrumentation. The stability analyzer was still capable of measuring the Allan variance and differential S-/X-band channel phase-stability parameters, and the results are included in this article.

Figure 15 depicts the total DSS-43 Radio Science System noise-power spectral density results with the X81 first LO input obtained from a hardline coaxial cable, using the substitute second LO, and operating the Test Transmitter on its DC power supply with output at X-band. The Voyager phase-noise specification is also shown, and since the noise-power spectral density is greater in magnitude than the phase-noise spectral density, the system meets the specification. It was determined that the 180-Hz spurious signal was contributed by the Fluke 6160 substitute synthesizer via the 5-MHz FTS reference signal; since the normal configuration utilizes the Dana which uses a 100-MHz reference signal, this spurious signal will not be present in the final system. Also shown in Fig. 15 is a broad-band spurious signal at 120 Hz.

Figure 16 is complementary to Fig. 15 and shows the spurious 120-Hz signal on an expanded horizontal axis. The figure shows a peculiar modulation-type signature which is unique to DSS-43 since this type of spurious signal was not visible in the DSS-45 spectrum. Figure 17 shows a similar noise-power spectral density measurement of the total Radio Science System at DSS-45. It lacks the 120-Hz spurious signal and meets the Voyager phase-noise specification. Figure 18 shows the DSS-45 Radio Science System noise-power spectral density measurements at S-band, which meet the phase-noise specifications.

Figure 19 depicts the initial test of the differential phase stability between the DSS-43 Radio Science System S- and X-band channels for a duration of one hour from 1430 to 1530 hours local time. The Test Transmitter was located within the X-band cone for connection to the X-band TWM, and the S-band output signal from the transmitter was connected via a sun-exposed coaxial cable to the S-band cone for connection to the TWM. The phase variation of approximately 16.5 degrees peak per hour is believed to be due to the sun-exposed cable since most of the phase-sensitive elements are the microwave assemblies of this experiment. For example, Fig. 20 shows the S-/X-band differential phase stability measurement conducted at DSS-45 where the transmitter and all connecting cables were located within the controlled environment of the cone. The measurement shows a 7-degree peak-per-hour variation for the same time duration.

Figure 21 depicts DSS-43 S-/X-band differential phase stability with the test signal radiated from the transmitter located on the roof of SPC-40 to the input of the DSS-43 antenna. The high, rapid phase variations are believed to be due to multipath effects. Only 10 minutes were available for this experiment and the variation of the mean of the plot is a 12-degree peak.

B. Usuda Tracking Station Test Results

After the JPL DAS was installed at Usuda, initial tests were performed to verify that the subsystem met pre-shipment acceptance test results. Figure 22 shows a performance shortfall that occurred immediately after installation. Here the phase-noise spectrum of the JPL DAS as measured with a 70-MHz IF test signal shows numerous 60-Hz harmonics spread beyond 2 kHz. This was a concern, even though the harmonics were below the S-band system specification of −45 dBc. The problem was traced to an improperly wired connection from the ISAS station 240/120-volt step-down power transformer to the JPL equipment; some power sockets were wired with reverse phase polarity. After correction of this anomaly, the JPL DAS repeated the acceptance test results. The extreme sensitivity of these radio science receivers required that the spurious signals be eliminated before performing further system tests.

While the correction of the improper wiring required considerable time, the majority of the test time was devoted to correcting the system to meet the Allan variance specification. The very long-term nature of the Allan variance test (1000-sec integration times) requires long test periods to obtain data with an acceptable confidence level. A typical test required 10 hours. The duration of the tests plus sensitivity of the system (even touching an exposed RF test cable affects

the results) meant that many days were required to isolate and correct the system before the specifications were finally achieved.

One major problem was the 5- to 100-MHz X20 frequency multipliers discussed previously. Initial and repeated measurements made with the ISAS X20 revealed a varying system performance in meeting the specification at 1-sec integration times. Figure 23 shows the typical performance of these units. The test configuration utilized the Test Transmitter and TWM provided by JPL, the ISAS RIVs and the ISAS DAS.

The spare X20 unit met the specification as shown in Fig. 23 with little margin; however, it was connected externally with extra cable lengths for testing, not installed in the normal cabinet drawer of the ISAS DAS. These tests indicated that the ISAS units produce marginal performance. The units use a 100-MHz quartz-crystal oscillator phase-locked to the 5-MHz reference input, and it is possible that they are susceptible to temperature fluctuations in the long term and induced vibrations in the short term.

The ISAS frequency-multiplier drawer was designed to accept either a 100-MHz reference signal directly or the normal 5-MHz reference signal. Thus, substituting the 100-MHz signal generated by the JPL unit was easy to accomplish for these tests. The JPL X20, located in the remote FTS room, consistently performed better than the two ISAS units which were located in the main control room together with the two data acquisition subsystems. The Allan variance of the JPL unit is shown in Fig. 24 using the JPL DAS. It was found during these tests that the use of either DAS had virtually no effect on the system Allan-variance results. The figure also shows a curve indicating the system Allan variance measured at the output of the NBOC digitizer's DAC. At this output test port the video signal has been sampled and represents the final level of degradation to the input RF signal. The curve indicates a small degradation relative to the NBOC input plot as expected from the sampling, and the entire system meets the specification with adequate margin.

A phase variation versus time plot of the downconverted test signal can be extracted from the measured raw Allan-variance data. Since the phase of the video signal depends on the phase of the local oscillators and the phase of the RF test signal, the data can be used to determine the phase performance of the LOs. Figure 25 shows the phase plot of the data used to construct Fig. 24, i.e., the system Allan variance using the JPL X20. The periodic nature of this curve suggests a strong temperature sensitivity in the LO chain. Note that the effect of a phase oscillation with period T is to increase the Allan variance at integration times on the order of T. In other words, the "plateau" on the Allan variance curve at 1000 seconds is due to the periodic fluctuations shown on the phase plot.

Figure 26 shows the Allan variance of the Usuda system taken with the ISAS X20. This is the same configuration used for Fig. 23, with the poorer of the two ISAS units. However, during this test a temperature probe was placed inside the ISAS DAS frequency-multiplier drawer. In Fig. 27, the recorded temperature results are compared with the phase plot derived from the Allan variance data, showing a strong correlation between temperature fluctuations in the LO frequency-multiplier drawer and the system phase. A change in temperature of 1 degree centigrade yields a change in phase of about 45 electrical degrees. However, this does not completely indicate that the ISAS X20 is the source of the temperature sensitivity, since the X97/100 and X94/100 modules are also present in this drawer. The first LO has a larger multiplication factor than the second LO and should be the major contributor. To isolate the source, additional testing will be necessary.

The plots described above demonstrate that a temperature sensitivity exists in the LO chain. This sensitivity causes an increase in the Allan variance at long integration times but does not degrade the system past the specified level. What has not been determined is the cause of the instability of the ISAS X20 at low integration times, and this is currently being investigated by ISAS personnel.

The Allan variance proved to be a more difficult parameter to meet than the phase-noise spectral density. This is mainly due to the relaxed specification for S-band systems (–45 dBc/Hz from 1 Hz to 10 kHz) because of the lower received SNR at S-band. The anticipated problems with power-line spurious signals did not materialize after the power connections were wired correctly.

Figures 28(a), 28(b), and 28(c) show the system phase noise measured using the JPL test transmitter and TWM, the ISAS RF-IF converter, and the JPL DAS. In this configuration, the original ISAS X20 was used. The plots are taken from an FFT spectrum analyzer and show the phase noise on the downconverted 20-kHz carrier over three different video-band frequencies: 0 to 50 Hz, 0 to 0.5 kHz, and 0 to 10 kHz. These frequencies correspond to the modulation frequency of the phase-noise component; thus, 0 Hz is right on the carrier. However, any DC component showing in the plots is purely an artifact of the phase-locking instrumentation used to demodulate the phase noise from the carrier. In general, the data on the plots are valid from the third or fourth FFT frequency bin and higher.

Figure 28(a) shows the phase noise to be about −55 dBc/Hz at f_m = 1 Hz and diminishing at higher frequencies. Figure 28(b) shows several 60-Hz and harmonically related spurious signals that reach a maximum of −56 dBc at 60 Hz, while the noise-spectrum magnitude levels off at about −75 dBc/Hz. Figure 28(c) shows the phase noise out to 10 kHz dropping to about −80 dBc/Hz. Because the resolution bandwidth is so high at 10 kHz, it is necessary to step across the 10-kHz band using smaller frequency spans to make sure no spurious signals are buried in the noise. In summary, the phase noise using the ISAS X20 meets specification with a margin of greater than 10 dB.

Because the JPL X20 is used as the backup to provide the 100-MHz signal for the LO chain, the system phase noise was measured using this unit. Figures 29(a), 29(b), and 29(c) show the phase noise over the video band of 0 to 50 Hz, 0 to 0.5 kHz, and 0 to 10 kHz. In Fig. 29(a), the phase noise at 1 Hz is approximately −63 dBc/Hz, dropping to about −79 dBc/Hz at 50 Hz. The 60-Hz spur shown in Fig. 29(b) is at about −61 dBc, with the noise-spectrum remaining flat at a level of −83 dBc/Hz. Finally, the noise in Fig. 29(c) is seen to decrease to −95 dBc/Hz at 10 kHz and level off.

Caution should be used if any conclusion is to be derived in comparing the merits of these two X20s from the sets of data since the RF test signal level used in the JPL X20 measurement was 14 dB higher than the level used for the ISAS unit. This was not deliberate, but resulted from a procedural error and explains the approximately 15-dB difference in the noise spectra levels in the region near 10 kHz (Fig. 28c compared to Fig. 29c).

These plots illustrate the combination of the phase-noise spectral density, resulting from the LO chain dominating at the low offset frequencies which are independent of the input RF test amplitude and exhibit a decreasing magnitude versus increasing offset-frequency spectrum distribution characteristic, and the input thermal-noise temperature spectral density which exhibits a nearly flat distribution and is dependent upon the test signal amplitude. This can be seen when comparing Fig. 28(c) to Fig. 29(c) near 6 kHz where the thermal noise is flat beyond 6 kHz and is the dominant contributor, since the phase noise due to the LO is gradually decreasing in this higher frequency region. Below 6 kHz the phase noise becomes the dominant contributor and increases in magnitude towards the low offset frequencies; thus, the plots of Fig. 28(a) and Fig. 29(a) can be considered mainly phase noise due to the LOs. The relative magnitudes of the phase noise shown in Figs. 28(a) and 29(a) can be used to compare the merits of the two X20s. The ISAS unit develops phase noise 8 dB higher at 1 Hz and tends to correlate with the degraded Allan variance performance at the 1-sec integration time relative to the JPL unit.

In summary, the Usuda Radio Science System meets the phase noise specification regardless of which X20 frequency multiplier is used. However, both the Allan variance and phase noise data indicate that the ISAS X20 is less stable than the JPL unit at integration times of about 1 sec. In order to meet the system Allan variance specification, the ISAS X20 needs to be improved. The JPL X20s are to be used as backups.

VI. Conclusion

The Voyager-Neptune encounter has levied very stringent requirements on the phase-noise spectral density characteristics and frequency stability of the DSN Radio Science Systems at Canberra and Usuda to ensure high performance at Neptune. The DSN has met these requirements with new designs in the signal-acquisition system and in test instrumentation. The results of tests conducted at Canberra and Usuda indicate that the design indeed meets the performance requirements.

References

[1] G. L. Tyler, "Radio Propagation Experiments in the Outer Solar System with Voyager," *Proceedings of the IEEE*, vol. 75, no. 10, pp. 1404–1430, October 1987.

[2] E. H. Sigman, "Phase Calibration Generator," *TDA Progress Report 42-92*, vol. October–December 1987, Jet Propulsion Laboratory, Pasadena, California, pp. 89–104, February 15, 1988.

[3] D. W. Allan, "Time and Frequency (Time-Domain) Characterization, Estimation, and Prediction of Precision Clocks and Oscillators," *IEEE Trans. on Ultrasonics, Ferroelectric and Frequency Control*, vol. UFFC-34, no. 6, November 1987.

[4] C. A. Greenhall, "A Method for Using a Time Interval Counter to Measure Frequency Stability," *TDA Progress Report 42-90*, vol. April–June 1987, Jet Propulsion Laboratory, Pasadena, California, pp. 149–156, August 15, 1987.

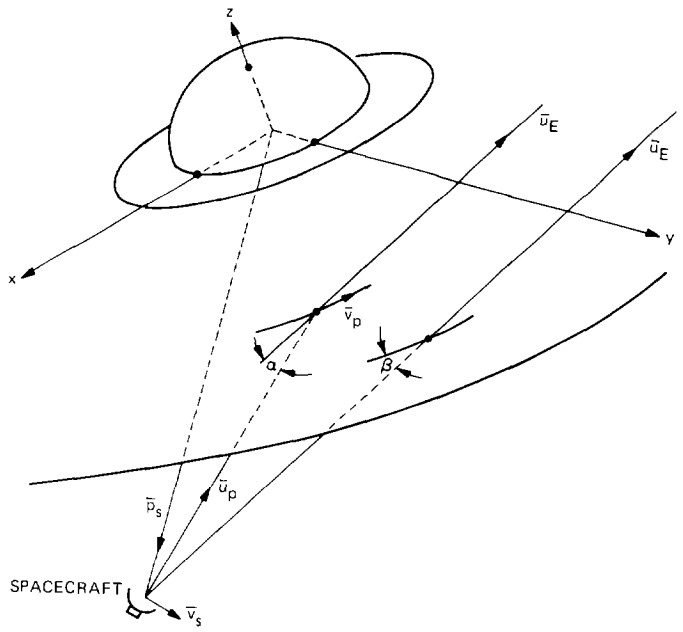

Fig. 1(a). Geometry of ring occultation, signal on direct and indirect path to Earth.

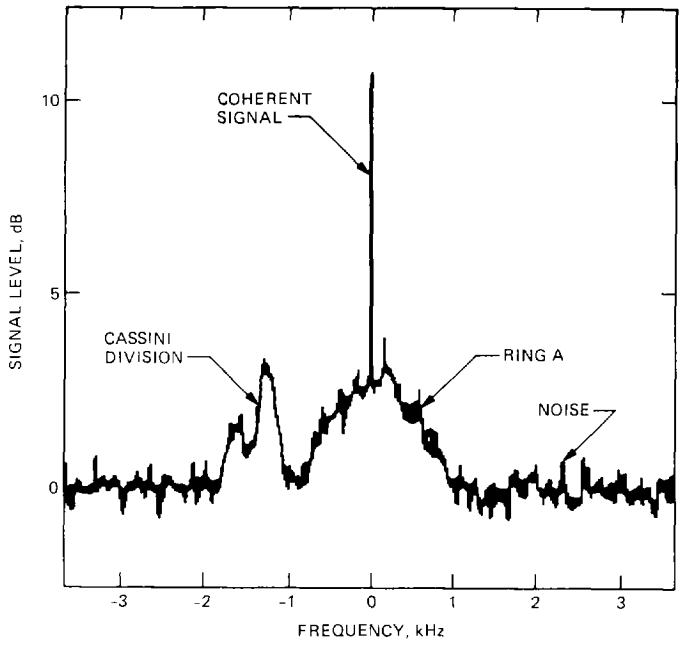

Fig. 1(b). Spectrum of received signal when Voyager 1 was behind Saturn's Ring A. Central spike is the coherent direct path signal. Symmetrical broad spectrum ±1 kHz about spike is from ring-particle scattering; separate broad feature is from Cassini Division particles.

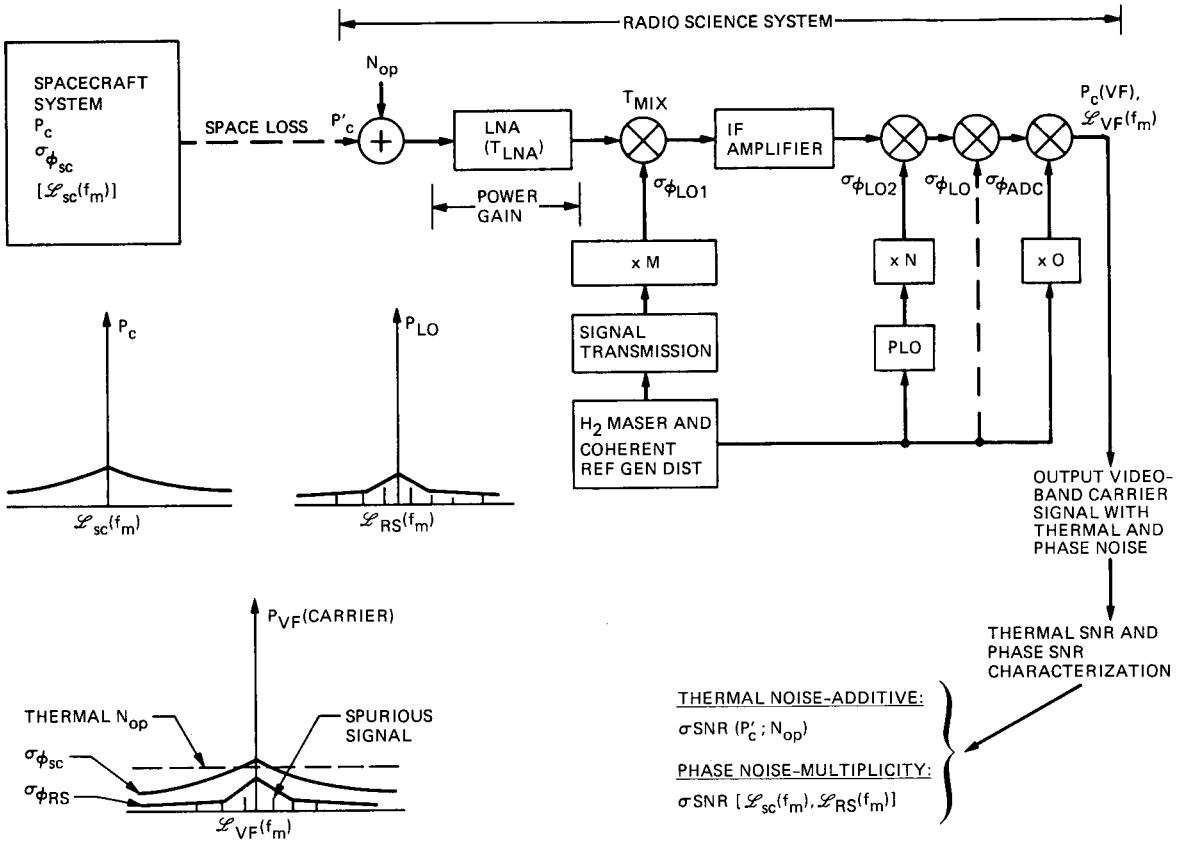

Fig. 2. Model of thermal and phase noise for the spacecraft and Radio Science System.

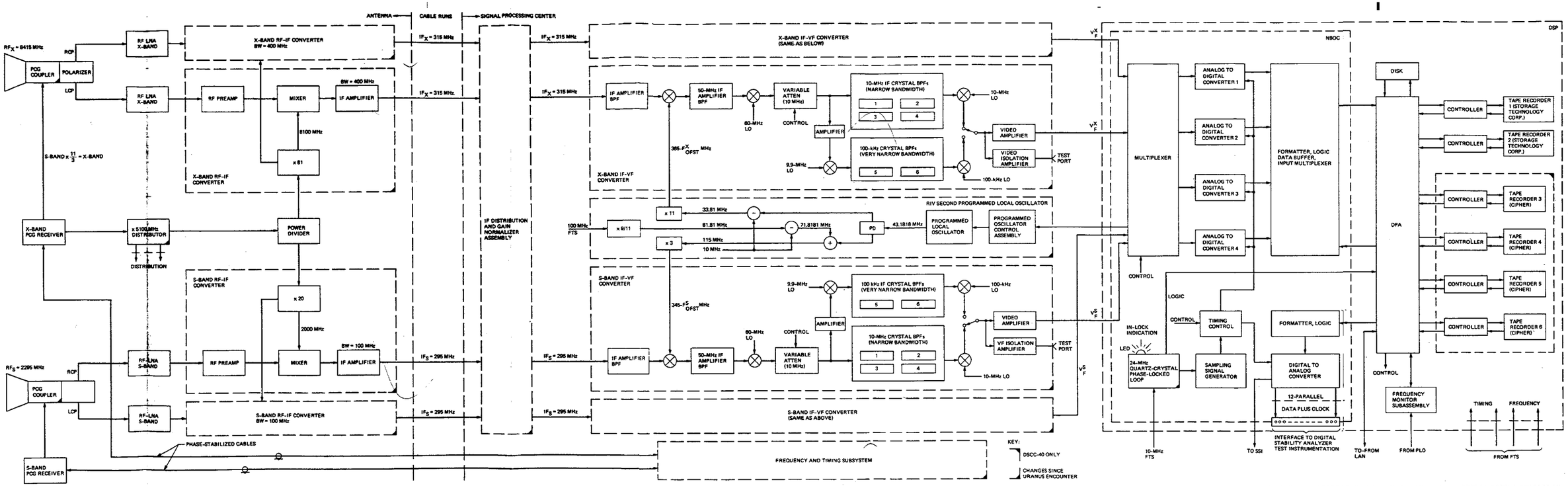

Fig. 3. Block diagram of DSCC I Radio Science System, 70-m antenna (DSCC-10, DSCC-40, and DSCC-60).

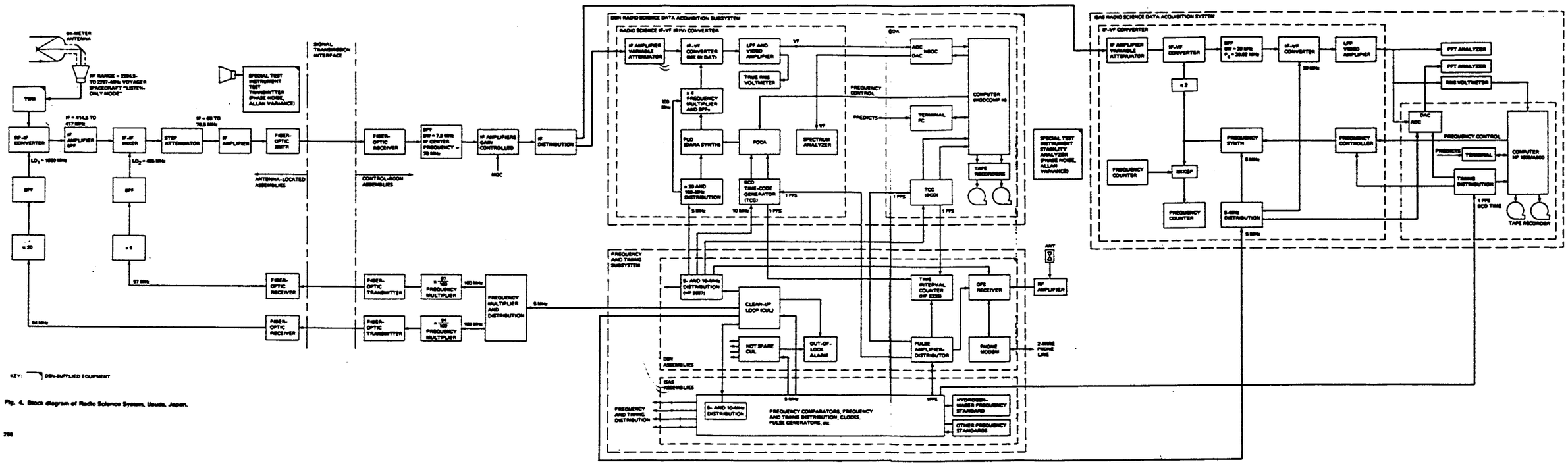

Fig. 4. Block diagram of Radio Science System, Usuda, Japan.

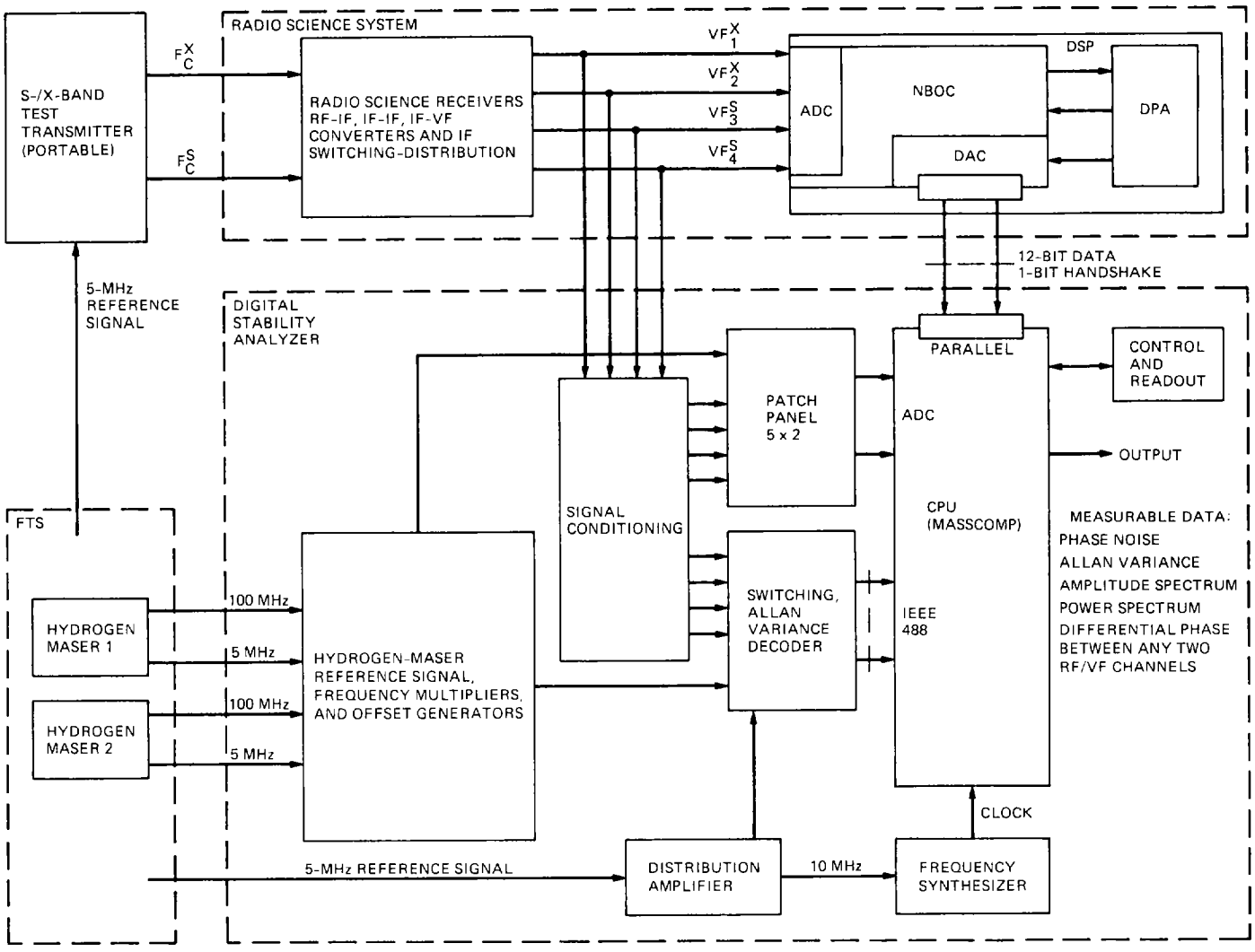

Fig. 5. Block diagram of Digital Stability Analyzer illustrating test methodology.

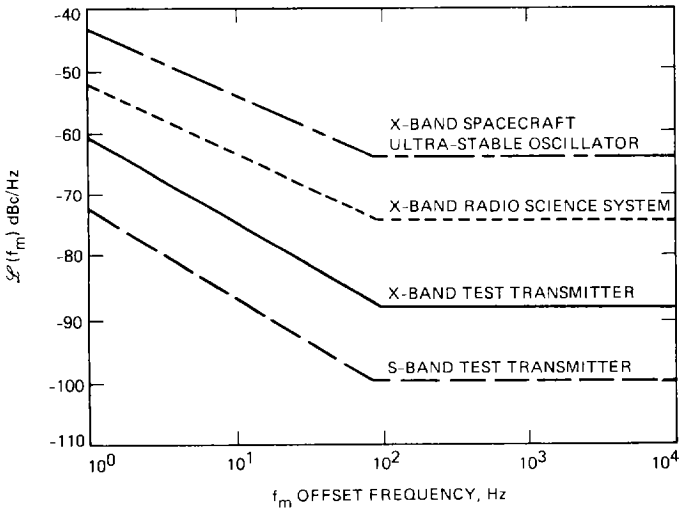

Fig. 6. Relative phase-noise spectral densities of future spacecraft USO, DSCC Radio Science System, and S-/X-band Test Transmitter.

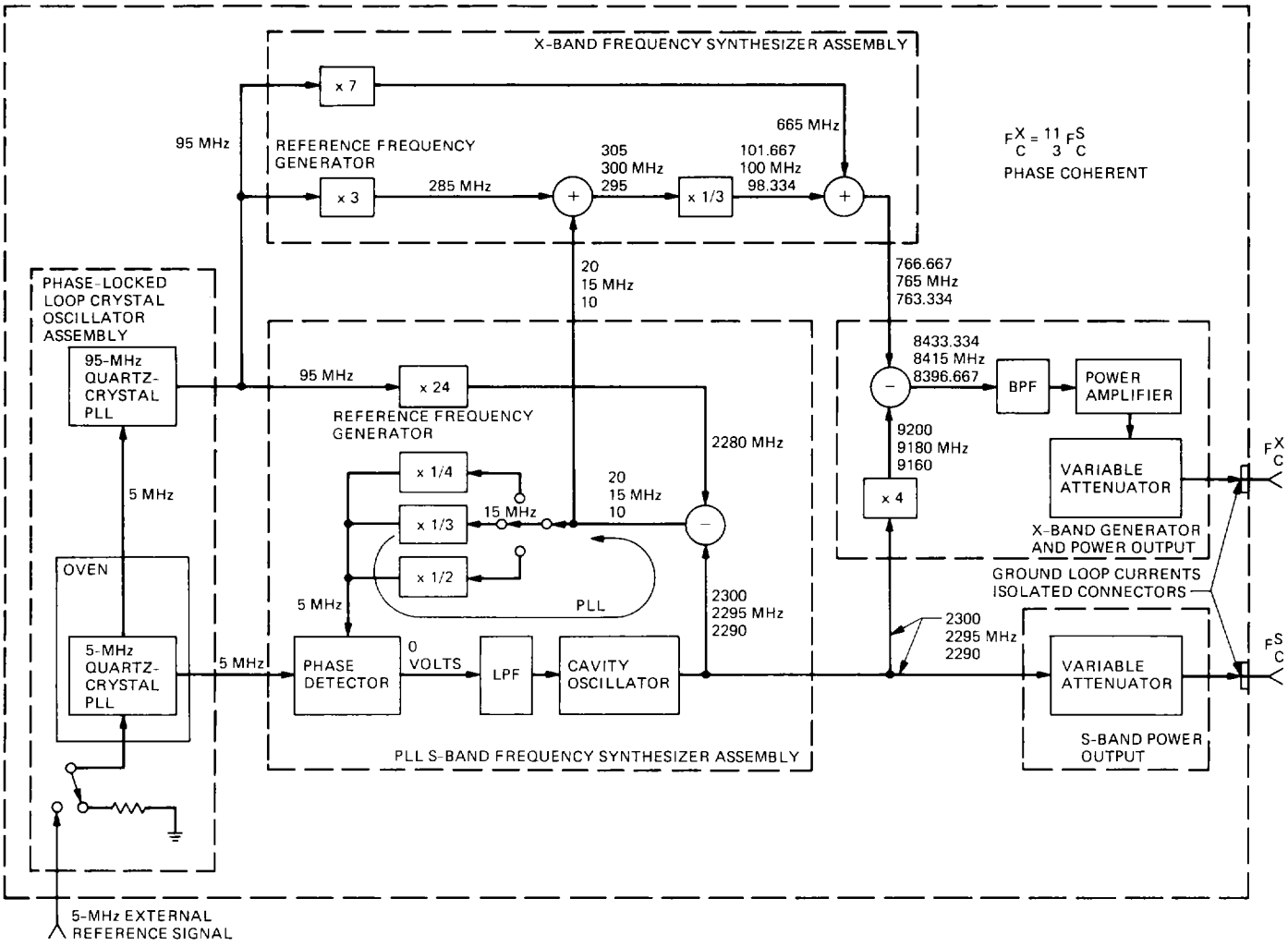

Fig. 7. S-/X-band Test Transmitter test instrumentation.

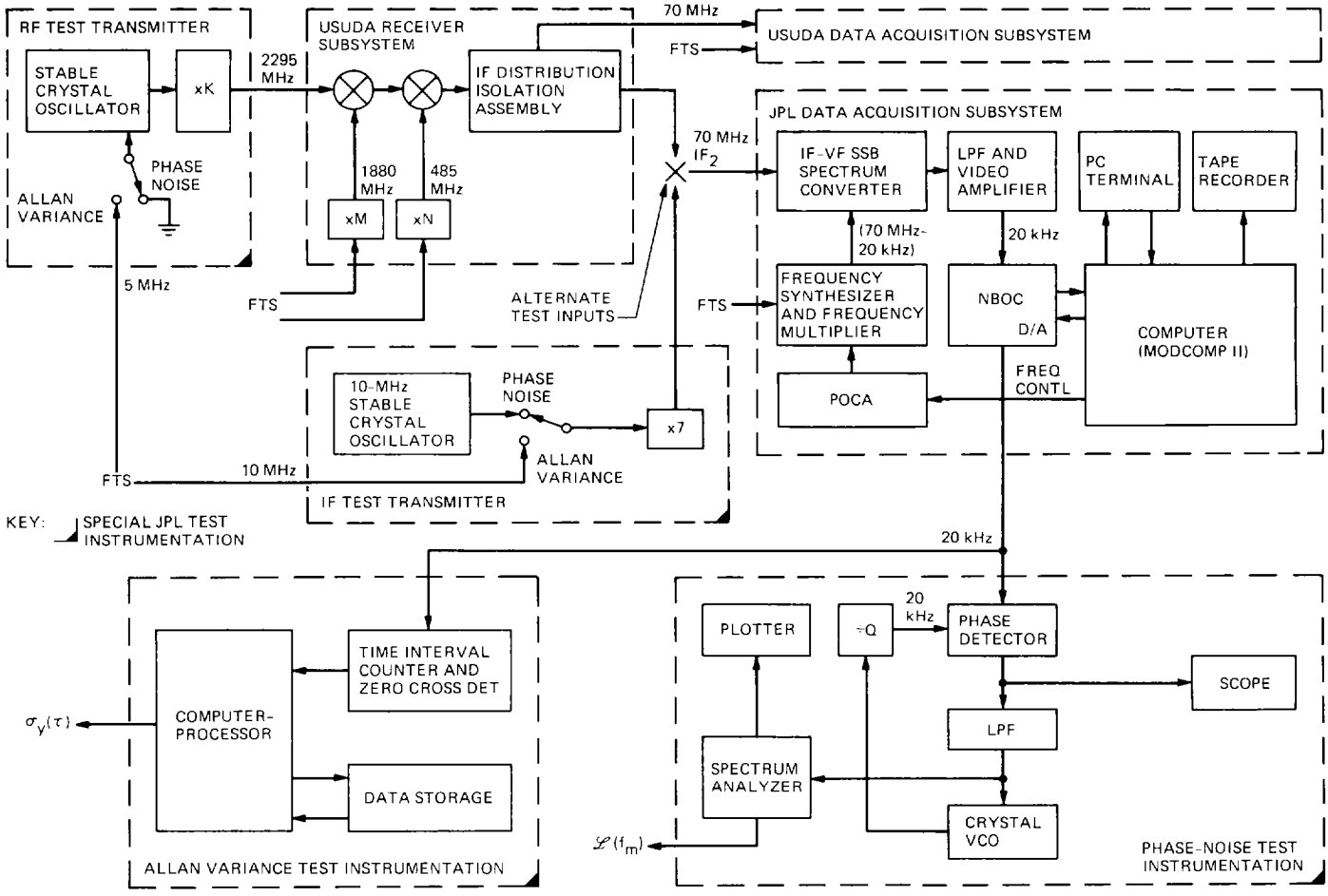

Fig. 8. Usuda test methodology and instrumentation.

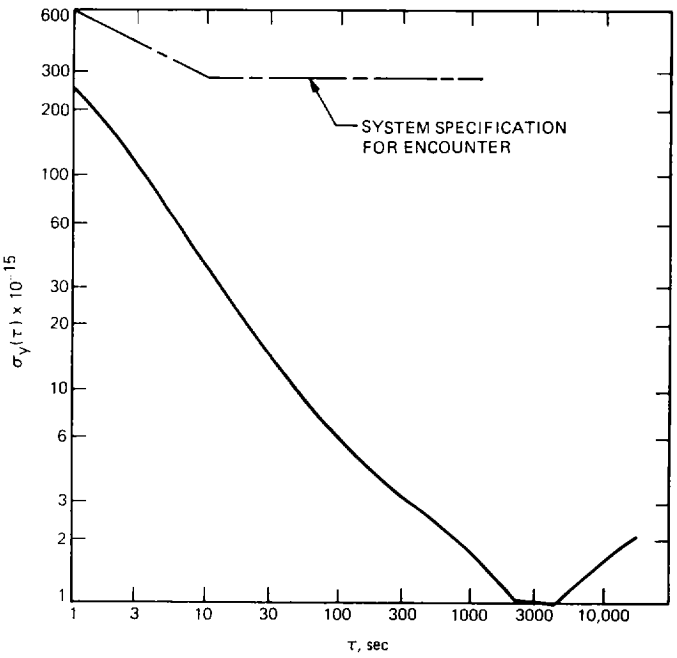

Fig. 9. Allan variance measurement of two hydrogen-maser frequency standards at CDSCC.

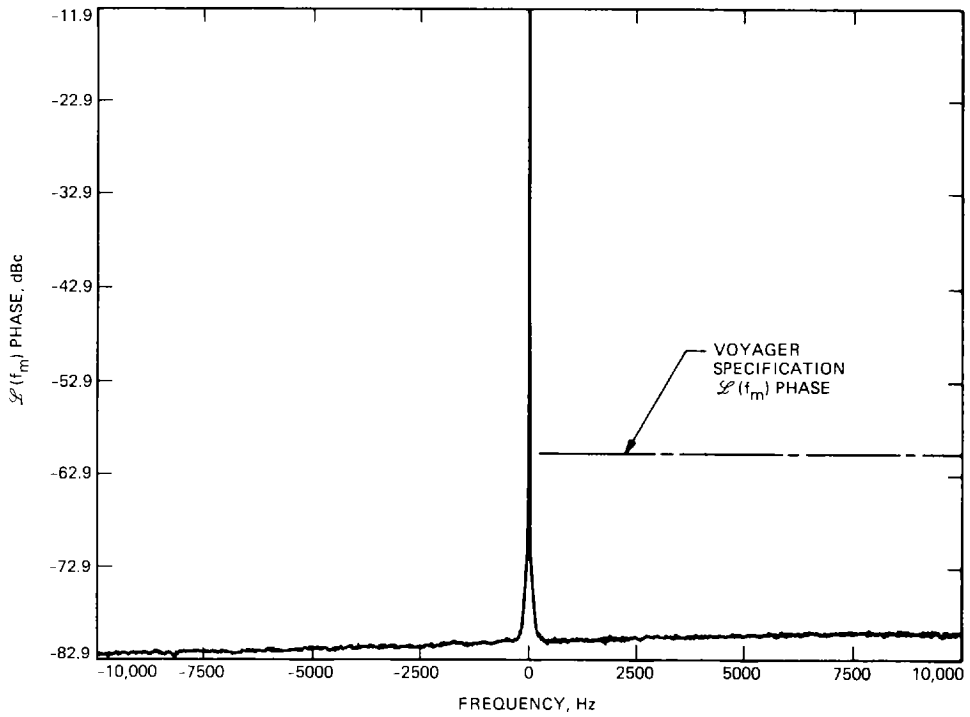

Fig. 10(a). Noise-power spectral density of two hydrogen masers at CDSCC, −10,000 to +10,000 Hz (center frequency = 10 GHz).

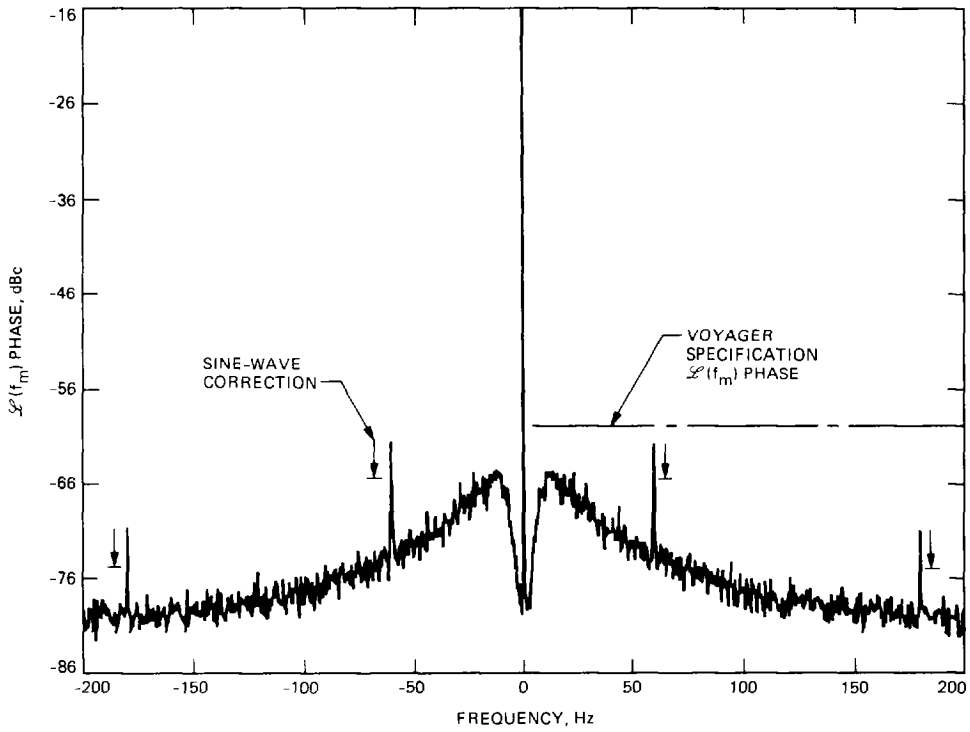

Fig. 10(b). Noise-power spectral density of two hydrogen masers at CDSCC, −200 to +200 Hz (center frequency = 10 GHz).

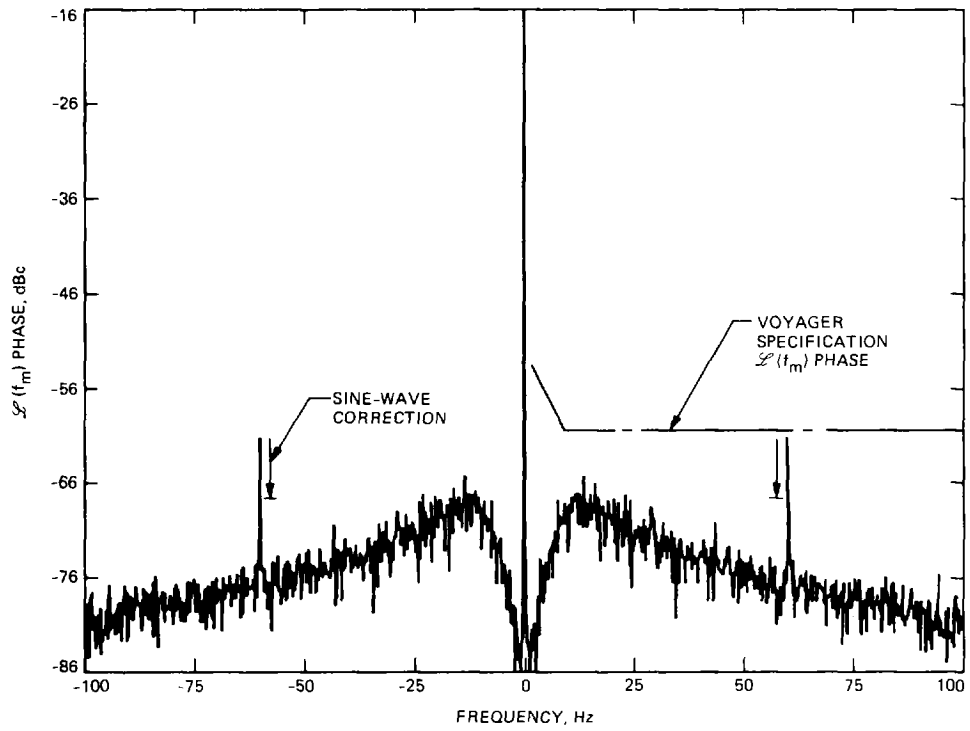

Fig. 10(c). Noise-power spectral density of two hydrogen masers at CDSCC, −100 to +100 Hz (center frequency = 10 GHz).

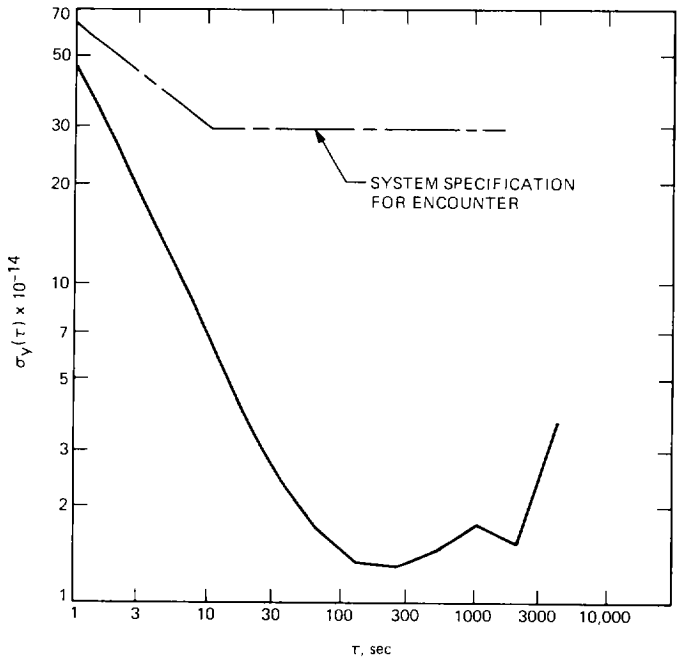

Fig. 11. Allan variance measurement of DSS-43 Radio Science System at X-band (Test Transmitter locked to PCG, 20 MHz × 1/4).

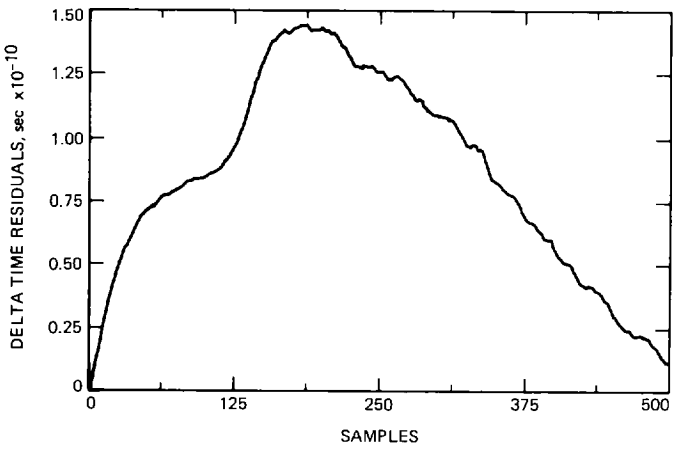

Fig. 12. Allan variance time-residual plot of CDSCC hydrogen masers.

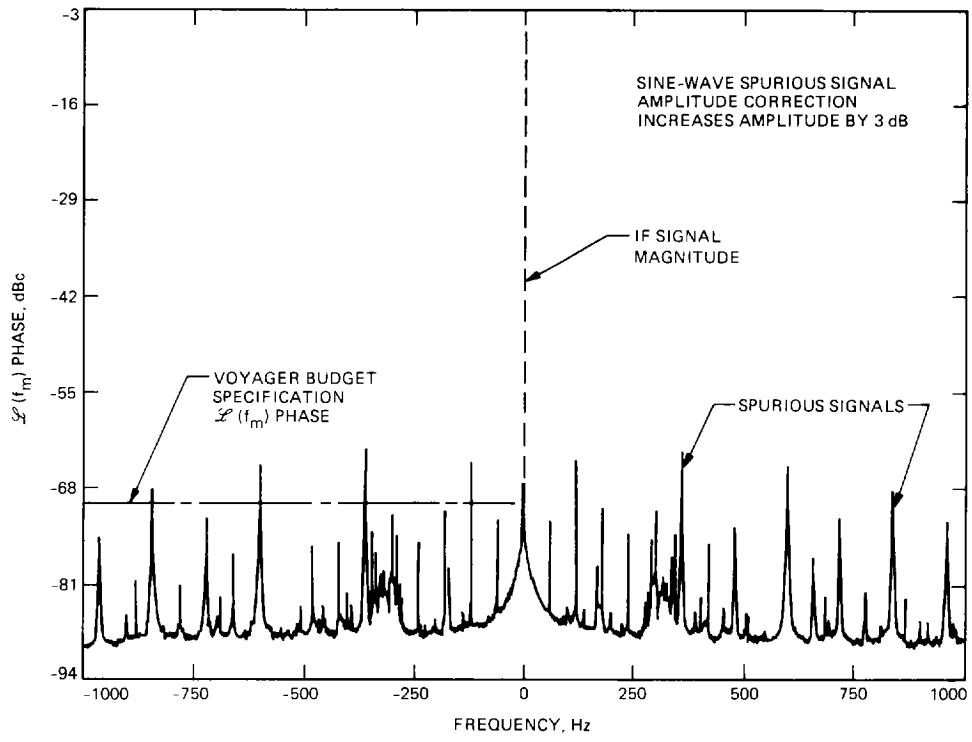

Fig. 13. Phase-noise spectral density of SPC-40 radio science IF-VF converter (Dana POCA as second LO).

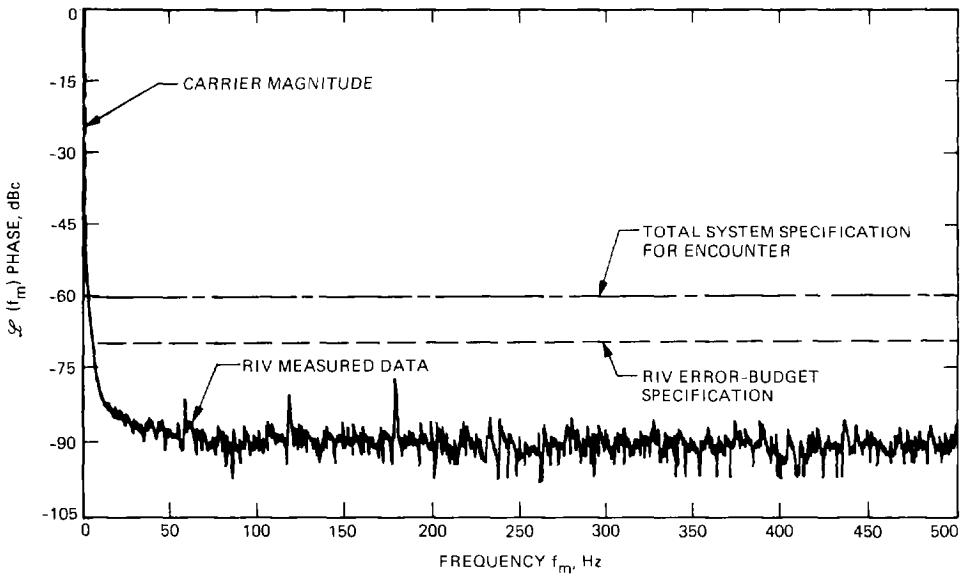

Fig. 14. Noise-power spectral density of CDSCC radio science IF-VF converter (Fluke 6160 as substitute second LO).

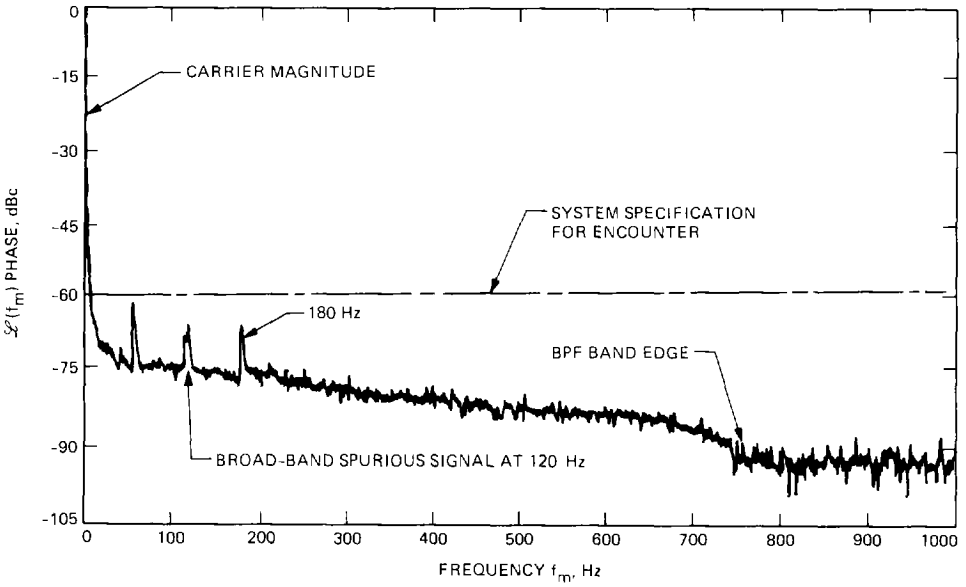

Fig. 15. Noise-power spectral density at X-band, DSS-43 Radio Science System (Fluke 6160 as second LO).

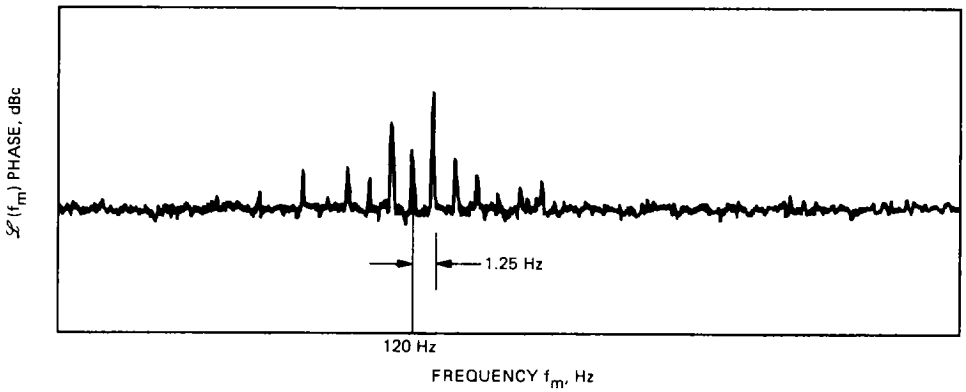

Fig. 16. Unique spurious signal at about 120 Hz, DSS-43 Radio Science System.

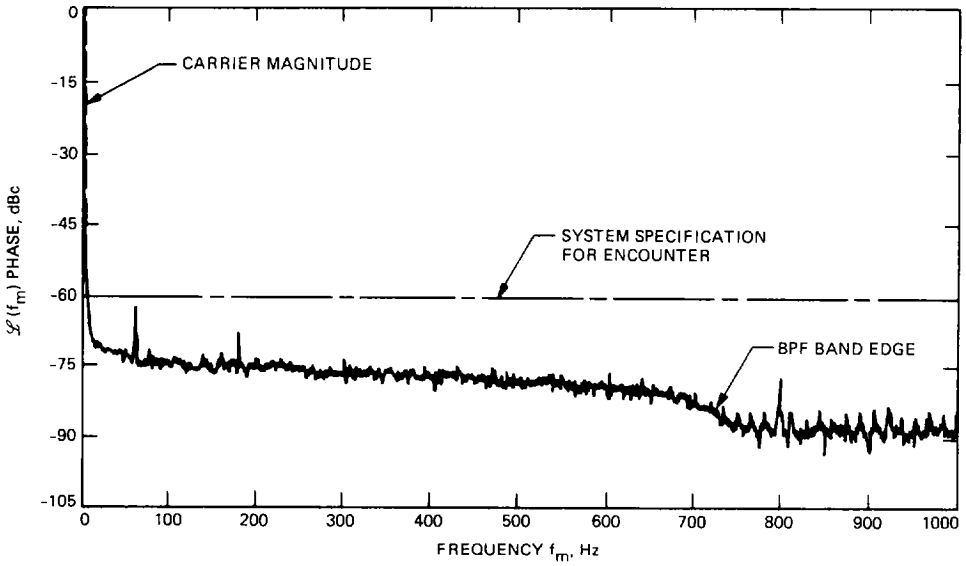

Fig. 17. Noise-power spectral density at X-band, DSS-45 Radio Science System (Fluke 6160 as second LO).

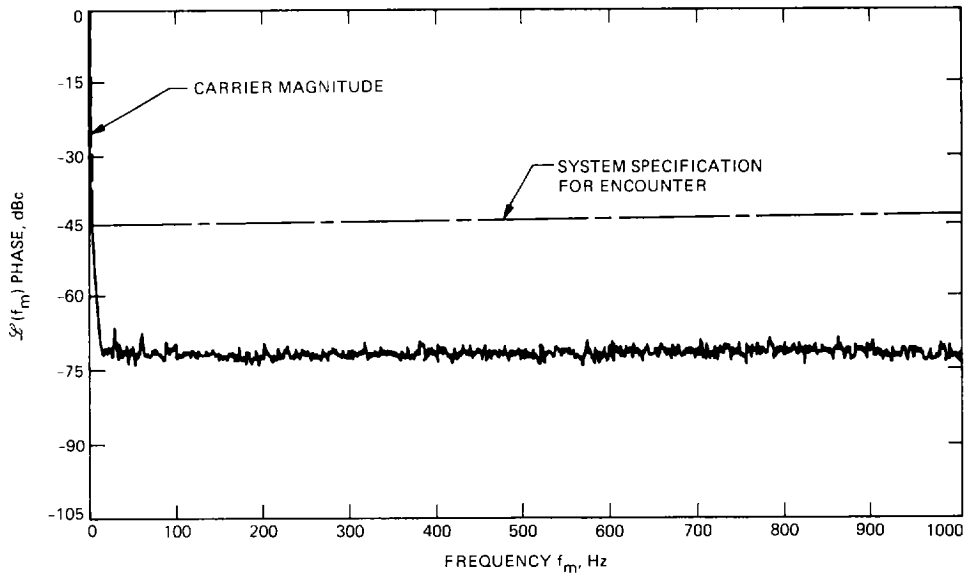

Fig. 18. Noise-power spectral density at S-band, DSS-45 Radio Science System (Fluke 6160 as second LO).

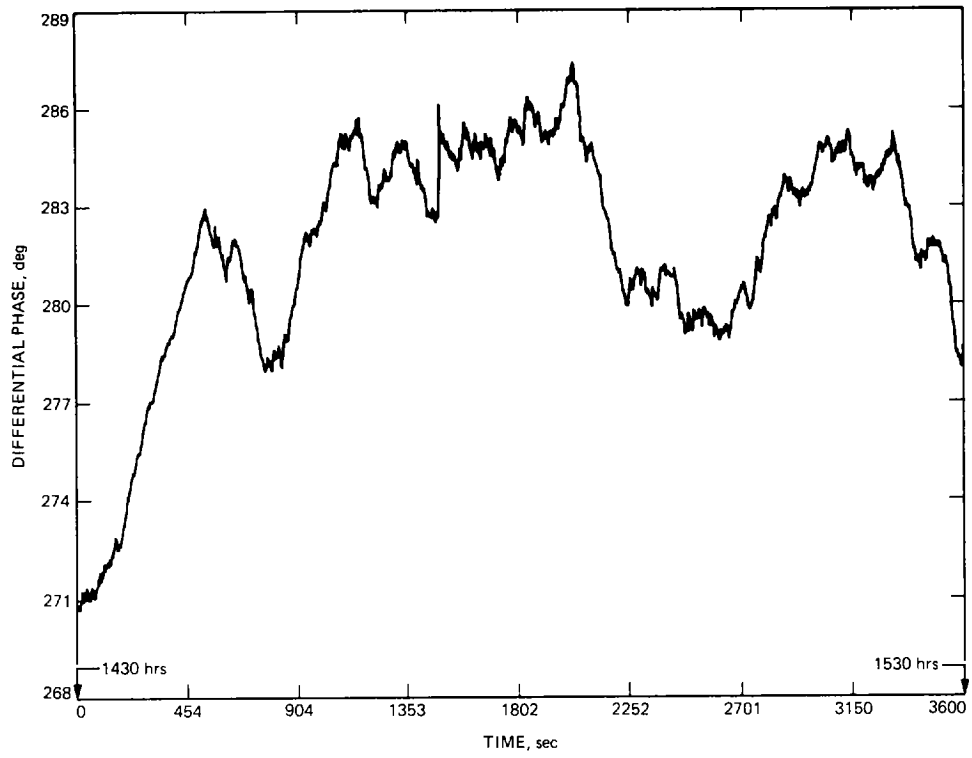

Fig. 19. S-/X-band differential phase stability, DSS-43 Radio Science System.

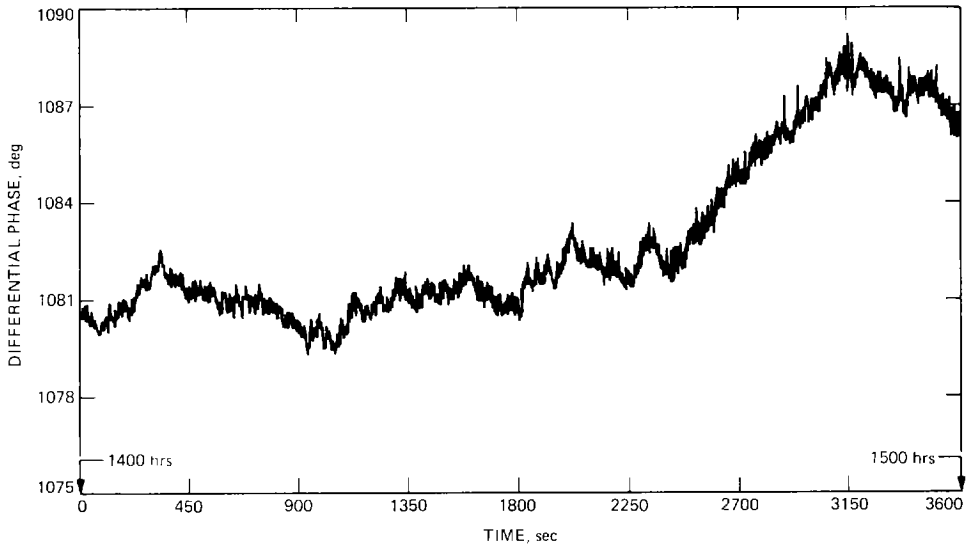

Fig. 20. S-/X-band differential phase stability, DSS-45 Radio Science System.

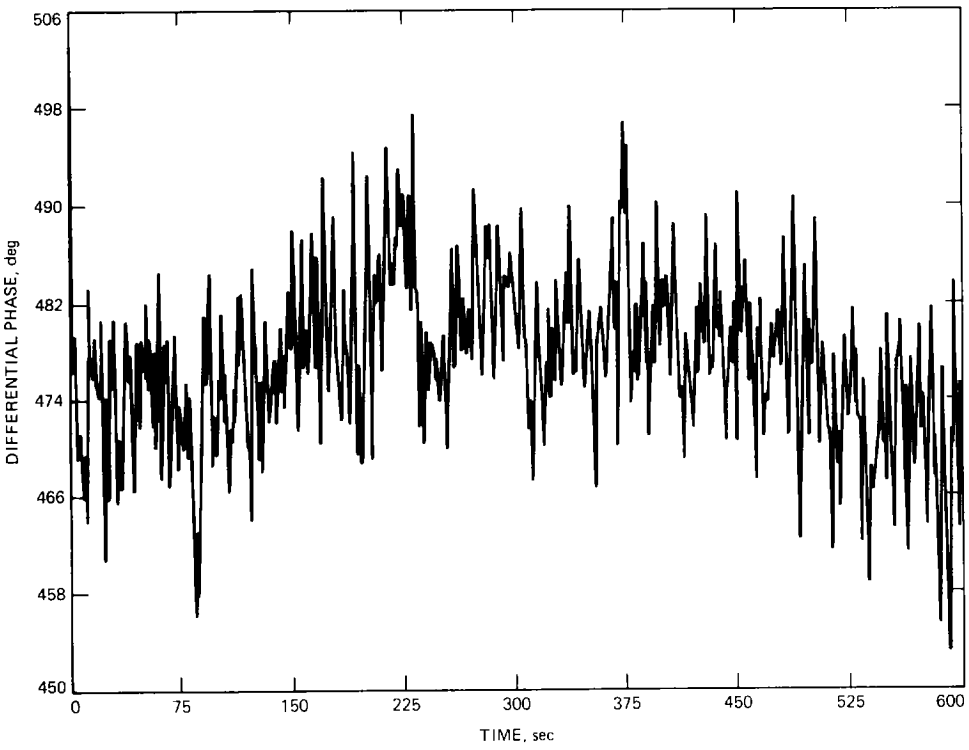

Fig. 21. S-/X-band differential phase stability of DSS-43 Radio Science System with test transmitter signals radiated to the antenna.

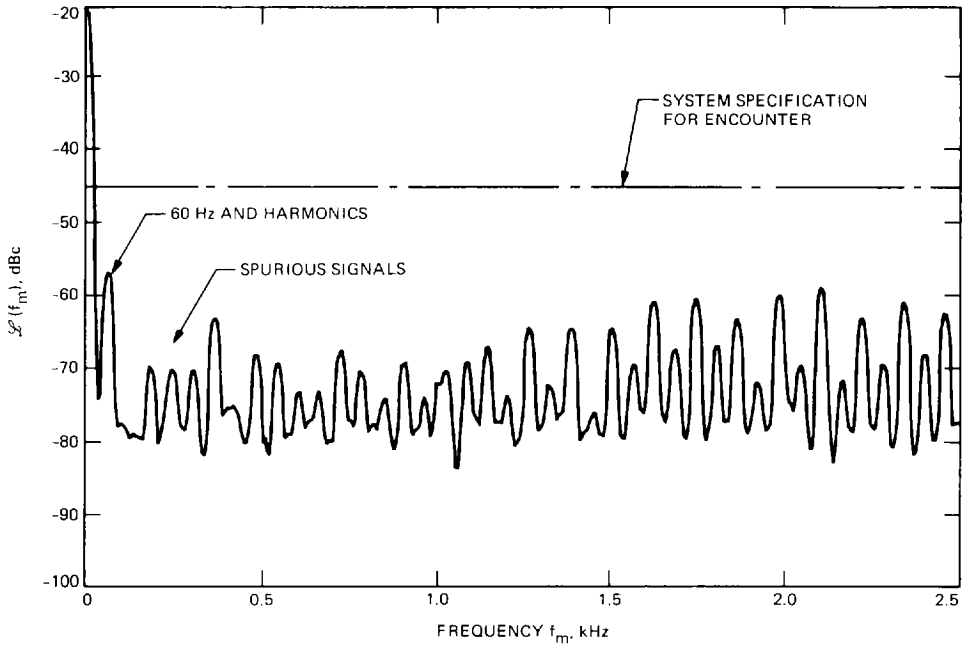

Fig. 22. Spurious signals in phase noise of the JPL DAS at Usuda due to improperly wired power connections.

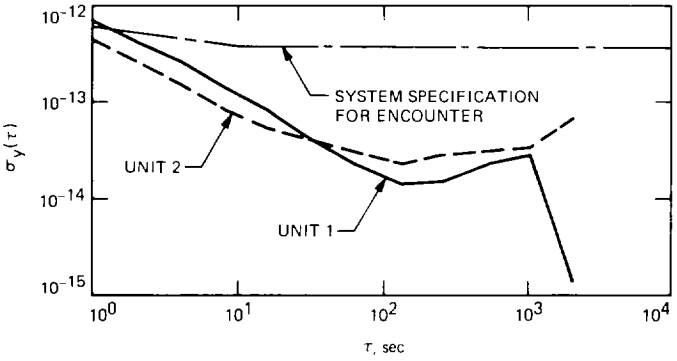

Fig. 23. Allan variance of the Usuda system using two × 20 frequency-multiplier units provided by ISAS.

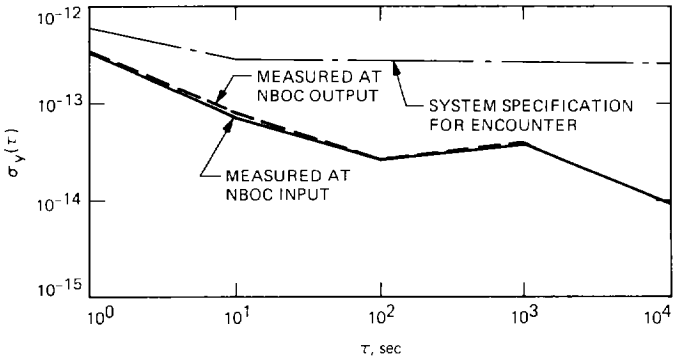

Fig. 24. Allan variance of the Usuda system using the JPL × 20 frequency-multiplier unit, measured at the NBOC input and NBOC output.

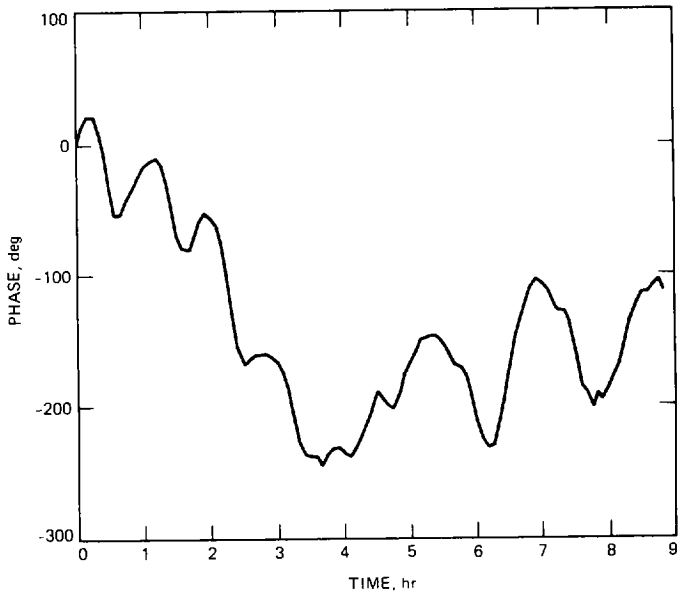

Fig. 25. Phase variation versus time plot, Usuda system, using the JPL × 20 frequency-multiplier unit.

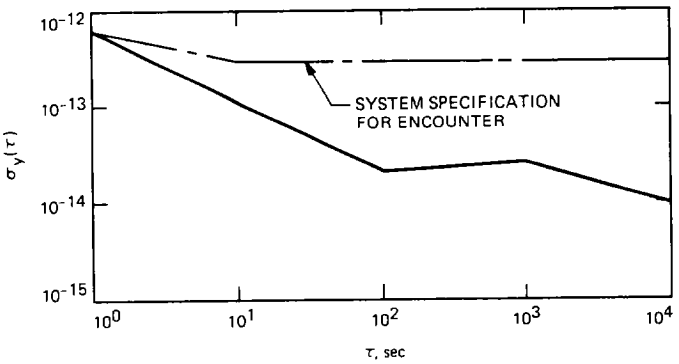

Fig. 26. Repeat measurement of Allan variance, Usuda system, using ISAS Unit 1 × 20 frequency-multiplier unit with temperature measurement.

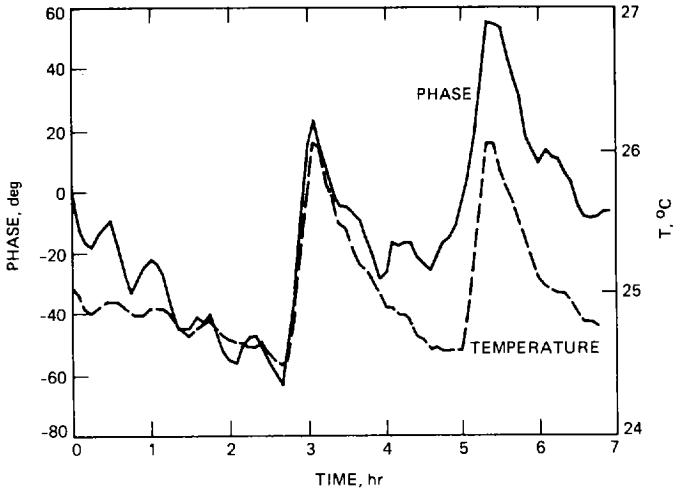

Fig. 27. Phase variation versus time compared to the ISAS × 20 frequency-multiplier unit temperature measurement, Usuda system.

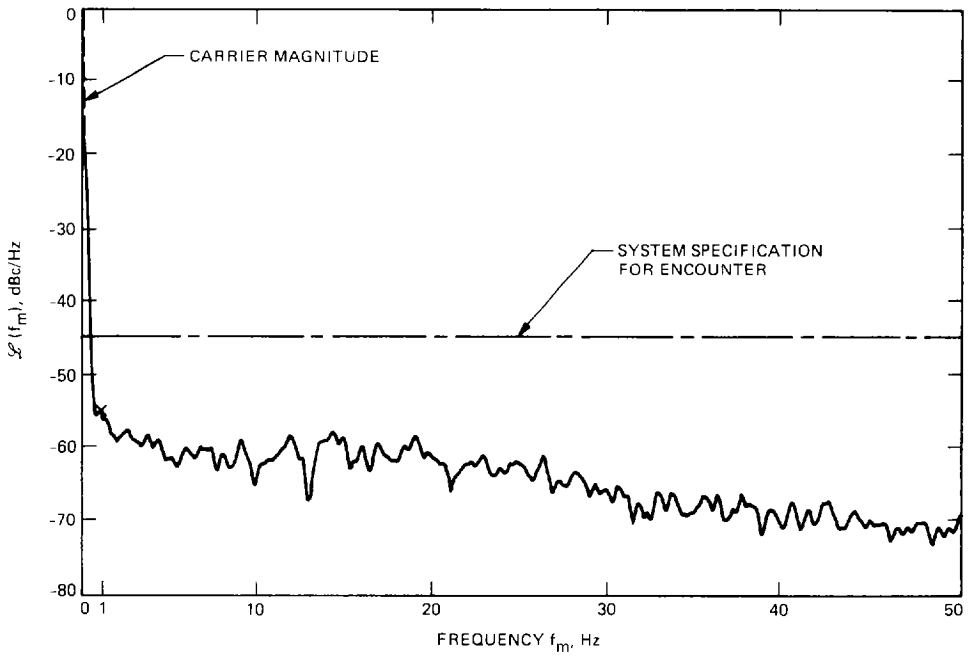

Fig. 28(a). Phase-noise spectral density of the Usuda Radio Science System (0 to 50 Hz, ISAS × 20 assembly in LO chain).

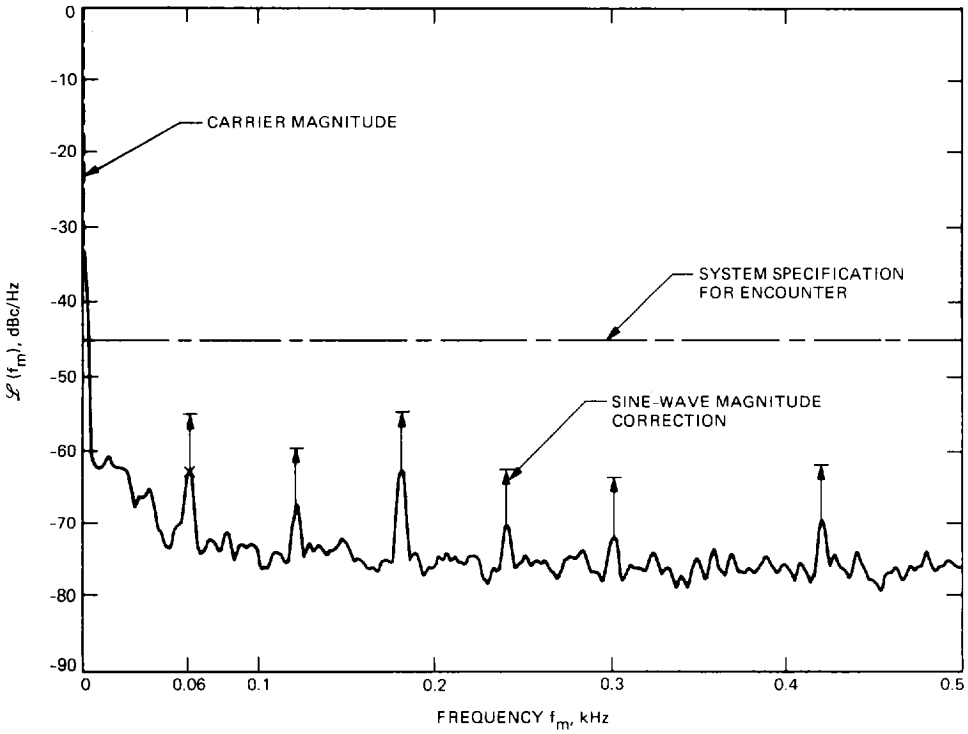

Fig. 28(b). Phase-noise spectral density of the Usuda Radio Science System (0 to 0.5 kHz, ISAS × 20 assembly in LO chain).

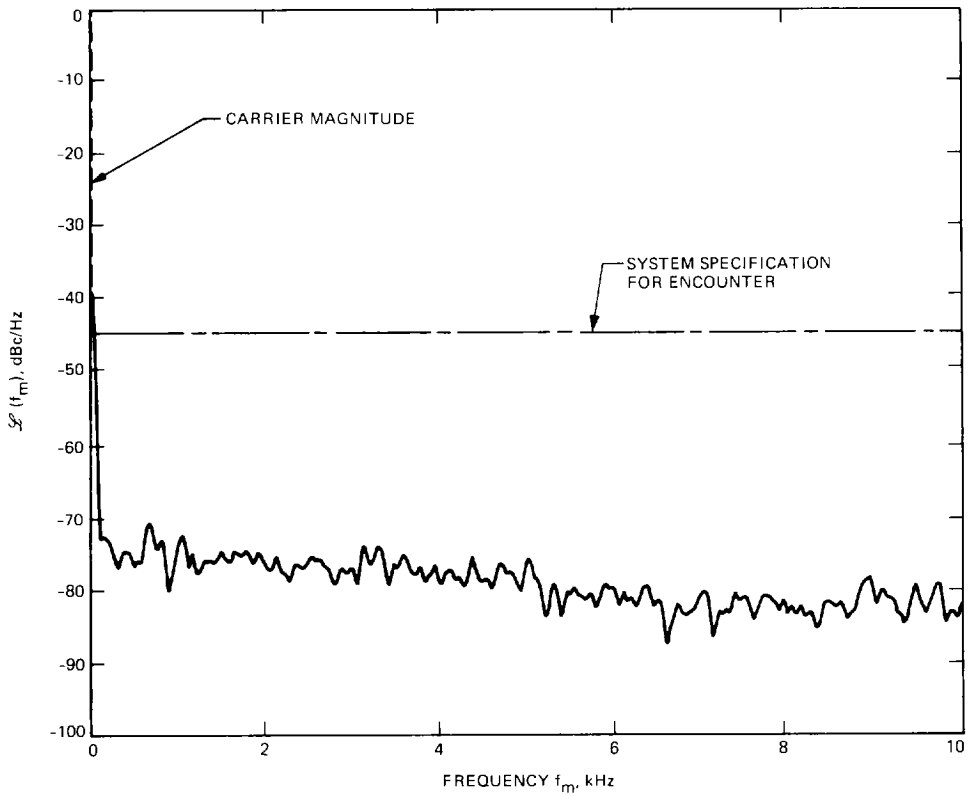

Fig. 28(c). Phase-noise spectral density of the Usuda Radio Science System (0 to 10 kHz, ISAS × 20 assembly in LO chain).

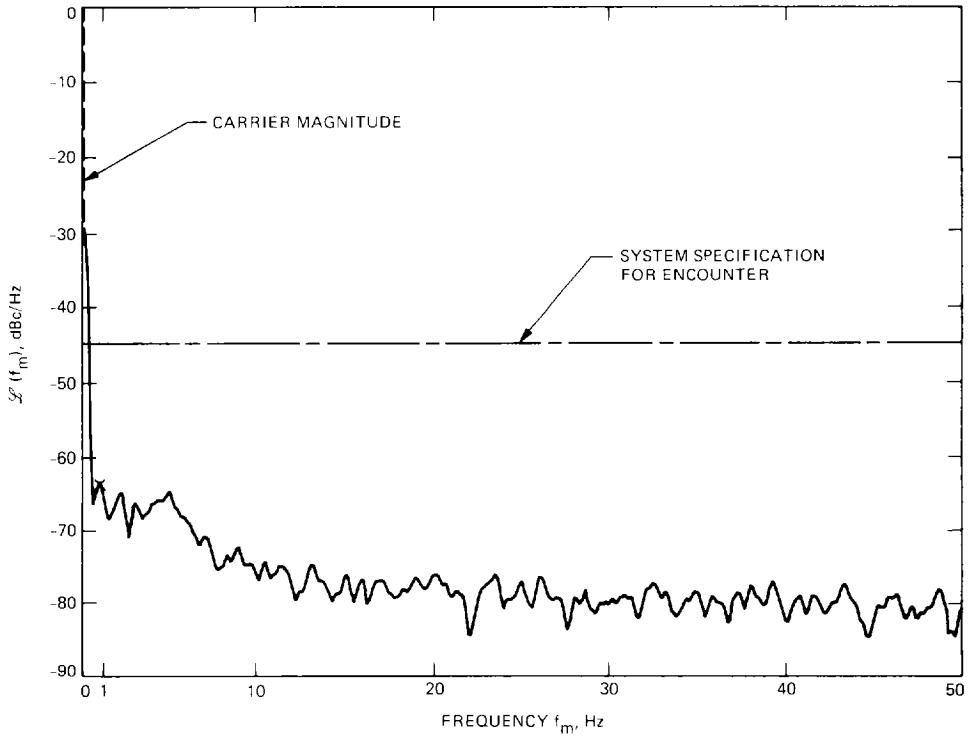

Fig. 29(a). Phase-noise spectral density of the Usuda Radio Science System (0 to 50 Hz, JPL × 20 assembly in LO chain).

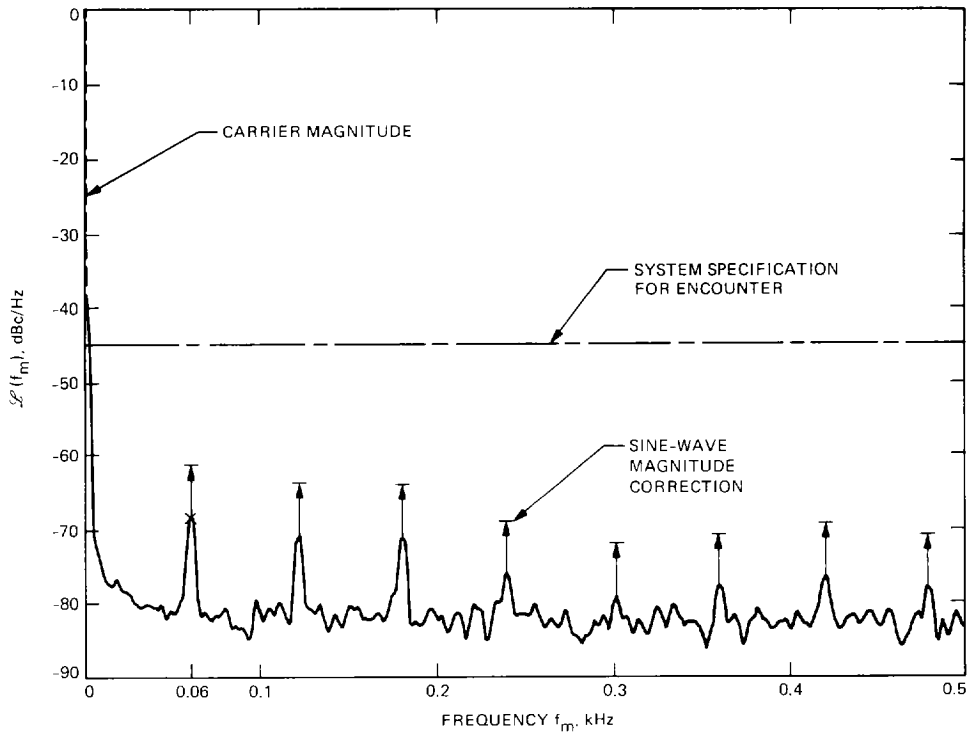

Fig. 29(b). Phase-noise spectral density of the Usuda Radio Science System (0 to 0.5 kHz, JPL × 20 assembly in LO chain).

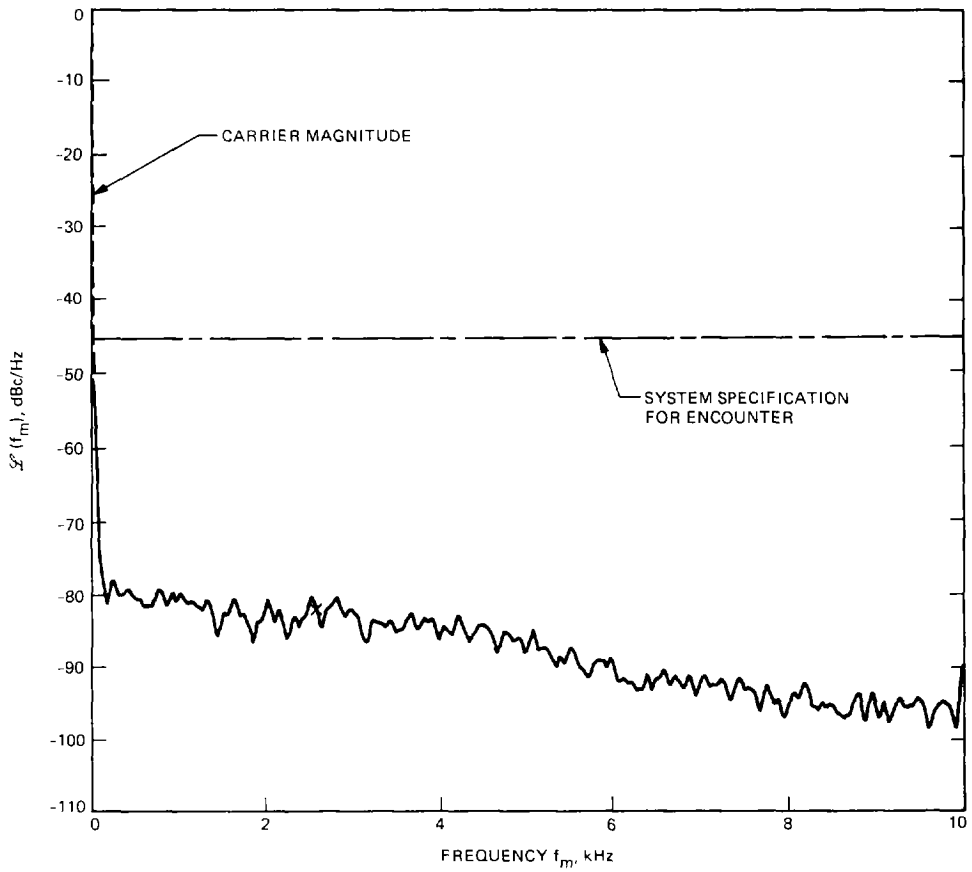

Fig. 29(c). Phase-noise spectral density of the Usuda Radio Science System (0 to 10 kHz, JPL × 20 assembly in LO chain).